

No breakdown of the radiatively-driven wind theory in low-metallicity environments^{*†}

J.-C. Bouret^{1‡}, T. Lanz², D. J. Hillier³, F. Martins⁴, W. L. F. Marcolino⁵, E. Depagne⁶

¹ Aix Marseille Université, CNRS, LAM (Laboratoire d'Astrophysique de Marseille) UMR 7326, 13388, Marseille, France

² Laboratoire J.-L. Lagrange, UMR 7293, Université de Nice-Sophia Antipolis, CNRS, Observatoire de la Côte d'Azur B.P. 4229, 06304 Nice Cedex 4, France

³ Department of Physics and Astronomy & Pittsburgh Particle physics, Astrophysics, and Cosmology Center (PITT PACC), University of Pittsburgh, 3941 O'Hara Street, Pittsburgh, PA 15260, USA

⁴ LUPM-UMR5299, Université Montpellier II & CNRS, Place Eugène Bataillon, F-34095 Montpellier Cedex 05, France

⁵ Universidade Federal do Rio de Janeiro, Observatório do Valongo, Ladeira Pedro Antônio, 43, CEP 20080-090, Rio de Janeiro, Brazil

⁶ South African Astronomical Observatory (SAAO), Observatory Road Observatory Cape Town, WC 7925, South Africa

Received 2014 December 18 – Accepted 2015 February 19

ABSTRACT

We present a spectroscopic analysis of HST/COS observations of three massive stars in the low metallicity dwarf galaxies IC 1613 and WLM. These stars, were previously observed with VLT/X-shooter by Tramper et al. (2011, 2014) who claimed that their mass-loss rates are higher than expected from theoretical predictions for the underlying metallicity. A comparison of the FUV spectra with those of stars of similar spectral types/luminosity classes in the Galaxy, and the Magellanic Clouds provides a direct, model-independent check of the mass-loss – metallicity relation. Then, a quantitative spectroscopic analysis is carried out using the NLTE stellar atmosphere code CMFGEN. We derive the photospheric and wind characteristics, benefiting from a much better sensitivity of the FUV lines to wind properties than H α . Iron and CNO abundances are measured, providing an independent check of the stellar metallicity. The spectroscopic analysis indicates that $Z/Z_{\odot} = 1/5$, similar to a SMC-type environment, and higher than usually quoted for IC 1613 and WLM. The mass-loss rates are smaller than the empirical ones by Tramper et al. (2014), and those predicted by the widely-used theoretical recipe by Vink et al. (2001). On the other hand, we show that the empirical, FUV-based, mass-loss rates are in good agreement with those derived from mass fluxes computed by Lucy (2012). We do not concur with Tramper et al. (2011, 2014) that there is a breakdown in the mass-loss – metallicity relation.

Key words: stars: early-type – stars: massive – stars: mass-loss – stars: wind – stars: fundamental parameters – galaxies: individual: IC1613, WLM

1 INTRODUCTION

Hot star winds are radiatively-driven by the transfer of photospheric photon momentum to the atmospheric material through absorption and scattering by spectral lines (Castor et al. 1975; Vink et al. 2001). The basic properties of stellar winds therefore depend on both the number of metal lines available to absorb photon momentum and on their ability to absorb (i.e., their optical thickness). CNO and intermediate elements are dominant line drivers for the outer supersonic part of the winds, while iron group elements are responsible for the inner, subsonic part where mass-loss rate is set

(Vink et al. 2001). The mass-loss rates, \dot{M} , of massive hot stars are therefore expected to depend on the metal content Z . Based on Monte-Carlo simulations using an extensive line list, Vink et al. (2001) established a theoretical relation, $\dot{M} \propto Z^{0.69 \pm 0.10}$. On the observational side, Mokiem et al. (2007) derived a relation for early-type stars in our Galaxy and in the Magellanic Clouds ($Z/Z_{\odot} = 0.5, 0.2$ for LMC and SMC, respectively), obtaining a relation $\dot{M} \propto Z^{0.83 \pm 0.16}$ that is consistent with the radiatively-driven wind theory.

These conclusions have been recently questioned by Tramper et al. (2011), who observed six O-type stars in galaxies with sub-SMC metallicities, $Z/Z_{\odot} = 1/7$ (IC 1613, WLM, and NGC 3109) with VLT/X-shooter. From the modeling of the optical spectrum, they derived mass-loss rates that are higher than the values expected from the theoretical relation for the stars metallicity. The derived mass-loss rates are more consistent with LMC-type metal abundances. Several uncertainties were investigated that could af-

* Based on observations made with the NASA-ESA *Hubble Space Telescope* (program GO 12867), obtained at STScI, which is operated by AURA, Inc., under NASA contract NAS 5-26555.

† Based on data products from observations made with ESO Telescopes at the La Silla Paranal Observatory under programme ID 085.D-0741

‡ E-mail: Jean-Claude.Bouret@lam.fr

fect these determinations, including the metallicity of the galaxies (measured from the O/H ratio) and the correction for nebular emission, or the influence of stellar multiplicity on the derived mass-loss rate by dilution or wind-wind collisions. None of the solutions considered by Tramper et al. (2011), however, could explain their unexpected findings. These original results have been further supported by the analysis of an extended sample of 10 stars (Tramper et al. 2014).

If confirmed, such a breakdown of the mass-loss rate scaling with metallicity would have dramatic consequences on the ultimate evolution of these objects, hence far more serious consequences than a “simple” revision of our general physical understanding of massive star properties. Indeed, the lower mass-loss rates that are predicted at low metallicities imply that the removal of angular momentum during a star’s evolution is substantially reduced at lower metallicities, increasing the effects of rotation, especially on mixing (Maeder & Meynet 2001). How to correctly treat the effects of rotation and metallicity on mass-loss and mixing is relevant to any field that needs to understand the life cycles and feedback of massive stars. These stars are the primary source of production of all elements heavier than O (except Fe), that they release in the interstellar medium via their stellar winds or when they explode as core-collapse supernovae. The chemical and dynamical evolution of galaxies is thus set by massive stars (Freyer et al. 2003). Another example is the collapsar model for long-duration gamma-ray bursts (Woosley 1993), which requires evolved massive progenitors with large amounts of angular momentum and mixing, possibly to the point of completely mixing the star to a homogeneous composition (Yoon & Langer 2005; Martins et al. 2013). Furthermore, the WR/O star ratio in classical single-star evolution models is also expected to be modified by the metallicity dependence of the winds: low-metallicity environments should produce less WR stars, which therefore impacts the number of type Ib/c supernovae (Meynet & Maeder 2005). On the contrary, should stronger winds prevail at low metallicity, this would imply lower numbers of collapsars, and of type Ib and Ic supernovae in the high-*z* Universe.

Tramper et al. (2011, 2014) based their analysis of the mass-loss rate mostly on the H α line. Several studies have shown that the sensitivity of H α is limited to winds with mass-loss rates greater than about $10^{-7} M_{\odot} \text{ yr}^{-1}$, and this line only shows core filling for mass-loss rates between 10^{-6} and $10^{-7} M_{\odot} \text{ yr}^{-1}$ (see e.g. Marcolino et al. 2009). Additionally, wind clumping was neglected, although the presence of clumps has been established even at low metallicities (see Puls et al. 2008, and refs therein). Tramper et al. (2011, 2014) argue, however, that they expect that their conclusions would remain unchanged, should clumping be included in the analysis. This statement is quite surprising since, H α being sensitive to the square of the wind density, neglecting clumping leads to overestimate the mass-loss rates by a factor $1/\sqrt{f}$ (where f is the volume-filling factor associated with clumping). This corresponds to factors of 3 to 10 that are of similar amplitude than the expected metallicity effect between a Galactic massive star and a counterpart with the exact same photospheric parameters in the SMC typically. This raises the question of the reliability of the optical diagnostic for mass-loss determination, as well as of the underlying metallicity adopted for the galaxies IC 1613, WLM and NGC 3109.

Far-UV (FUV) spectroscopy, on the other hand, is the adequate tool to fully address and resolve this outstanding issue of the dependence of hot, massive star mass-loss rates with metallicity. Spectroscopy in the 1150 – 1800 Å waveband provides many of the major wind line diagnostics, including the N v $\lambda\lambda$ 1238, 1242 doublet that is also temperature, abundance, and X-ray ionization

dependent, the C iv $\lambda\lambda$ 1548, 1550 doublet that is particularly useful to diagnose weak winds, and the Balmer alpha transition of He II (λ 1640) that provides an extremely valuable clumping and abundance diagnostic for stars with strong winds (Hillier et al. 2003). In addition, N iv λ 1718, Si iv $\lambda\lambda$ 1395, 1402 (also luminosity sensitive) and O v λ 1371, are also sensitive to the clumpy nature of the winds of early O stars. Many other useful diagnostics are also found in this spectral range, such as T_{eff} indicators from C, N, O, and Fe lines that can be used instead of the classical helium ionization balance (Heap et al. 2006). Several lines are also good indicators of CNO and iron abundances (e.g. Hillier et al. 2003; Bouret et al. 2003). The numerous iron lines (Fe III to Fe V) present in the FUV spectrum provide a direct measurement of the stellar metallicity.

The goal of the work presented here was to corroborate (or not) the breakdown of the mass-loss rate – metallicity relation at sub-SMC metallicities with FUV observations with HST/COS of the three brightest stars from the original study by Tramper et al. (2011). The paper is organized as follows: we present the observations in Sect. 2 and we discuss the spectra morphology in Sect. 3. We describe the model and method we used for the determination of the stellar parameters in Sect. 4; we present the results of this modeling in Sect. 5. Then, in Sect. 6, we discuss what the actual metallicities of the galaxies are, while a possible binary status for the targets is presented in Sect. 7. Systematic uncertainties in the mass-loss determinations are discussed in Sect. 8, and wind properties at low metallicity in Sect. 9. In Sect. 10, we discuss how the wind properties we derive compare to theoretical expectations. We summarize our conclusions in Sect. 11.

2 OBSERVATIONS

We used the Cosmic Origins Spectrograph (COS) onboard the Hubble Space Telescope (HST), to obtain high-resolution ($R \approx 20,000$) FUV spectra of the three brightest stars from Tramper et al. (2011), namely A13 and B11 in IC 1613 and A11 in WLM (see also Bresolin et al. 2006, 2007). Aside from their intrinsic brightness, other selection criteria were that *i*) IC1613-A13 is the only star in the Tramper et al. (2011, 2014) sample with a mass-loss rate (\dot{M}) consistent with the theoretical prediction; *ii*) A11 is one of the only two stars in Tramper et al. (2011) with a mass-loss rate unambiguously larger (\sim an order of magnitude) than predicted, but the other object is almost one magnitude fainter; *iii*) A11 and B11 are late-type O supergiants (\sim O9.5 I) with much cooler effective temperatures ($T_{\text{eff}} \approx 30,000$ K) than A13. Interestingly, \dot{M} for B11 could be compatible with theory within the errors. On the other hand, A11 is notably brighter than B11 (0.35 dex), has lower surface gravity (0.2 dex) and a higher mass-loss rate (0.6 dex), suggesting that it is more evolved than B11. Observing both stars in the FUV with HST/COS would allow us to further constrain their evolutionary properties and derive unambiguous values for the mass-loss rates and address the issue of clumping in low metallicity stars.

Our program GO 12867 (PI: T. Lanz) was granted 18 orbits. Each target was observed in a sequence of 6 science exposures with COS using gratings G130M (λ 1291, λ 1327) and G160M (λ 1577, λ 1623). This sequence provides coverage without gap of the FUV spectrum between 1132 and 1798 Å. Overlapping segments have been co-added to enhance the final signal-to-noise ratio (SNR). Thanks to the high efficiency of COS in the FUV and little extinction toward the host galaxies, we achieved typically $\text{SNR} \approx 25$ per resolution element, in 6 HST orbits for each target (2 orbits for G130M and 4 orbits for G160M; the latest grating covers the

C IV $\lambda\lambda 1548, 1550$ doublet and He II $\lambda 1640$). Informations about the targets, including UBVRI photometry and exposure times are summarized in Table 1.

COS spectra are flux-calibrated (see Massa et al. 2013, for details and limitations) providing the flux distribution in the FUV wavelength range. We shall use the spectral absolute fluxes, together with UBVRI photometry (Table 1) to construct spectral energy distributions (SEDs) and constrain the intrinsic stellar luminosity (see Sect. 4.1). It is possible, however, that the spectra of the three targets are affected by physical or line-of-sight, unresolved multiplicity. Indeed, the nominal primary science aperture of *COS* has a radius of 1.25 arcsec^1 . At the distances of IC1613 and WLM (cf. Table 1), this subtends a field of view with physical size of 9-12 pc across, several times the size of a cluster like R136 (e.g. Crowther et al. 2010).

On the other hand, the FUV range of a spectrum is dominated by the hottest objects. Shall hotter objects than the targets be in the *COS* entrance aperture, the spectra will generally present signs of contamination (e.g. lines from higher ionization stages) which is not seen (see Sect. 3). More importantly, if the stars are in binary systems and their mass ratios differ greatly from unity, then the derived physical properties reflect those of the primary².

Furthermore, ground-based observations with spatial resolution indicate that the two targets in IC1613 are isolated within the *COS* field of view. We note also that Tramper et al. (2011, 2014) found that their luminosities are compatible with those of (single) stars with same spectral type/luminosity class in the MCs (e.g. Massey et al. 2009). Therefore, we are confident that the physical parameters we can derive from the modeling of the FUV (+ optical) spectra truly reflects the properties of the targets. The situation is not as clear for WLM-A11, where a significant source of optical flux is present within a $2.5''$ diameter circle (hence the “a” subscript of the luminosity class) in optical images. Since the flux level in the FUV, plus the whole UBVRI photometry, is also quite high, it might indicate that this target is actually a binary system with components of similar spectral types (more exactly similar effective temperatures). We will come back on this point in Sect. 7.

We also retrieved the optical, VLT/*X-shooter* spectra of the three targets (first presented in Tramper et al. 2011) from the Phase 3 ESO archives. These spectra have been processed using version v2.2.0 of the *X-shooter* pipeline. We used the spectra obtained in the UVB (300–550 nm) and VIS (550–1020 nm) arms with slit width of $0.8''$ and $0.9''$, which provide a spectral resolving power $R = 6200$ and $R = 7400$, respectively. Typical SNR per resolution element in the UVB spectra are 25, 20 and 18 for IC 1613-A13, IC 1613-B11 and WLM-A11, respectively. In the VIS arm, SNR per resolution element ranges from 10 to 12.

Following Tramper et al. (2014), we corrected the spectra from the nebular emission in the Balmer lines (and He I for IC 1613-A13), with special care for the $H\alpha$ line, as this is the principal mass-loss diagnostic available in the optical. These spectra have been used in the modeling process to better constrain the photospheric parameters (especially T_{eff} and $\log g$) and to check how the synthetic $H\alpha$ profiles produced by FUV-based \dot{M} compare to observations.

¹ Note that the *COS handbook* (Holland et al. 2012) mentions that “the aberrated beam entering the aperture allows objects up to 2 arcsec from the center of the aperture to contribute to the recorded spectrum”

² But see R136A for a case not showing strong evidence, from spectroscopy and the SED, for binarity even though its a multiple system.

3 SPECTRA MORPHOLOGY

In a first step, we compared the *COS* spectra of IC 1613-A13, IC 1613-B11 and WLM-A11 with existing FUV spectra of SMC, LMC and Galactic stars of similar spectral type and luminosity class. In principle, this should provide a direct, qualitative, model-independent, indication about the mass-loss rate – metallicity relation. The line of reasoning is straightforward. The strength of a P Cygni profile is directly related to the optical depth of the wind in the corresponding line. The optical depth is related to the total number of absorbing ions in the transition giving rise to the spectral line and can be written as $\tau_{\text{rad}} \propto \dot{M} q_i A_E$ with A_E and q_i the abundance of element E and its ionization fraction for stage i. It is therefore readily seen that, for stars with similar physical properties and evolutionary stages (as should be for stars within the same spectral/luminosity classes), hence yielding similar ionization fractions, τ_{rad} scales with the mass-loss rate and the abundance (which is expected to scale with metallicity).

We selected stars with spectral classification as close as possible to those of IC 1613-A13, IC 1613-B11 and WLM-A11 although a perfect match was not always possible. Also, whenever possible, we chose stars with high resolution spectra, such that we can further compare the numerous lines from iron ions. High-resolution *IUE* spectra exist for Galactic massive stars of all spectral type and luminosity class. In the Magellanic Clouds (MCs), several *IUE* spectra are available but they have poor signal-to-noise ratios and were not considered for this comparison. In the MCs, good signal-to-noise high-resolution spectra have been obtained with HST but for a limited number of objects. For early-type dwarfs in the LMC, such good signal-to-noise high-resolution (Goddard High-Resolution Spectrograph, *GHR*S) spectra exist but they are restricted to stars in R136. These O-type stars often seem quite extreme objects in terms of stellar and wind parameters (de Koter et al. 1998; Prinja & Crowther 1998; Massey et al. 2004), in excess of those found for Galactic stars of similar spectral type (Bouret et al. 2005; Martins et al. 2012). We chose to use the spectrum of a field star instead, namely LH81W28-5, whose spectrum was obtained at low resolution though (G140L) with *STIS* (Massey et al. 2004). We could not find a high-resolution spectrum (*COS*, or *STIS* or *GHR*S) for LMC late-type supergiant and we had to rely on the more modest resolution provided by *FOS* for B1170; we use it for comparison to both IC1613-B11 and WLM-A11. We could find only one late-type supergiant in the SMC, namely AzV 327, with high-resolution (*STIS*) FUV spectrum. Here again, this star is used for comparison to B11 and A11. The IDs of the stars we used for the morphology comparisons are summarized in Table 2, together with additional indications about their FUV spectra, V-magnitude and reddening.

For the comparisons presented in Fig. 1 (B11 and A11) and Fig. 2 (A13), we used absolute fluxes, corrected for reddening, such that we avoid potential problems related to the choice of a continuum to rectify the spectra. Fluxes for Galactic, LMC and SMC stars have been scaled by the appropriate ratio to match the continua of the three targets in spectral regions of interest (i.e., around wind profiles). These scaling factors present relatively small deviation from those that would be obtained from a scaling to the distance modulus of IC 1613 and WLM as given in Tramper et al. (2011).

We first discuss the cases of IC 1613-B11 and WLM-A11 as they have similar spectral type/luminosity classes. Qualitatively, their behavior is easy to interpret in the framework of the line-driven wind theory. The top three panels in Fig. 1 show that the wind terminal velocity decreases with decreasing metal content,

Table 1. Basic parameters of our targets and exposure times of the *COS* spectra.

| Star | Sp. Type | <i>U</i> | <i>B</i> | <i>V</i> | <i>R</i> | <i>I</i> | $E(B - V)$ | dist. (kpc) | M_V | Texp (s) | |
|-------------|--------------|----------|----------|----------|----------|----------|------------|----------------|-------|----------|--------|
| | | | | | | | | | | G130M | G160M |
| IC 1613-A13 | O3-O4 V((f)) | 17.66 | 18.73 | 18.96 | ... | 19.26 | 0.03 | 721 | -5.42 | 4640. | 10006. |
| IC 1613-B11 | O9.5 I | 17.45 | 18.49 | 18.62 | ... | 18.78 | 0.08 | 721 | -5.92 | 4581. | 9927. |
| WLM-A11 | O9.7 Ia | 17.23 | 18.27 | 18.38 | 18.45 | 18.57 | 0.04 | 995 | -6.73 | 4625. | 9992. |

Note : Spectral types are from Tramper et al. (2011) and Garcia et al. (2014), while the photometry is taken from Garcia et al. (2009, 2014) for the stars in IC1613 and from Massey et al. (2007) for WLM-A11. Color excess $E(B - V)$ is calculated using the calibration by Martins & Plez (2006) for Galactic Stars. Absolute magnitude are calculated using the quoted distances to IC1613 and WLM from Pietrzyński et al. (2006) and Urbaneja et al. (2008) respectively.

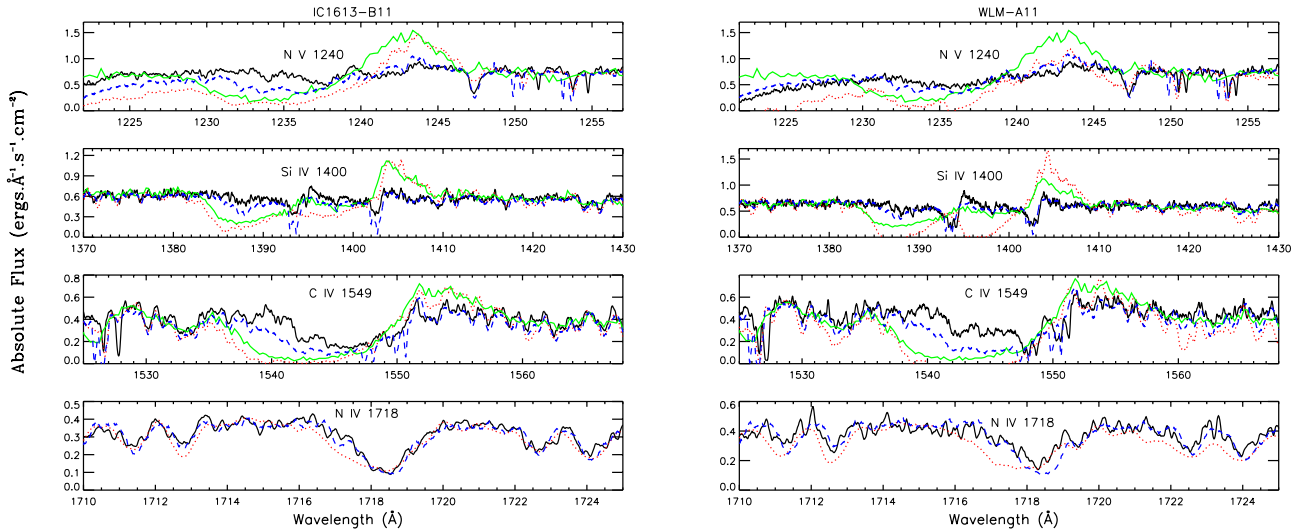


Figure 1. P Cygni profiles for B11 (left) and A11 (right) in black. Overplotted in red, green and blue are the spectra of the Galactic, LMC and SMC stars (respectively) chosen for comparison (cf. Table 2). For plotting purpose, the fluxes were scaled by a factor 10^{14} .

from Galactic to IC 1613/WLM, while the P Cygni profiles get simultaneously weaker. This especially clear for the second and third panels for each star, which demonstrate that this trend holds for the resonance doublets of Si IV and C IV. On the other hand, caution should be used concerning the N v resonance doublet at 1238, 1242 Å, which is notoriously sensitive to X-ray irradiation, that is not known for the stars used for this comparison. P Cygni profiles are well-defined for the Galactic and LMC stars but only a weak (if any) emission component is observed for the SMC star, as well as IC1613-B11 and WLM-A11. The C IV $\lambda\lambda$ 1548, 1550 profiles still show a blueward extension that is related to the wind whereas it is barely seen on the Si IV doublet because of the ten times lower abundance of Silicon versus Carbon. The panels showing N IV λ 1718 on the other hand, show very similar profiles for IC1613-B11 and WLM-A11 and their SMC counterpart, both weaker nevertheless than for the Galactic star of comparison. Overall, the morphology of the profiles from Fig. 1 seem to contradict the conclusion by Tramper et al. (2011) that IC1613-B11 and WLM-A11 have mass-loss rates higher than expected for their metallicity. This of course assumes that the line-driven wind theory holds for stars in the Galaxy and down to SMC metallicity, as checked by Mokiem et al. (2007).

It is also easily seen on Fig. 1 that the iron lines present in the FUV spectra of IC 1613-B11 and WLM-A11 (see e.g. the bottom two panels, Fe IV lines between $\lambda\lambda$ 1530–1570 and $\lambda\lambda$ 1710–1730) are moderately weaker, if at all, than those of the SMC star we chose for comparison, despite a slightly higher projected rotational

velocity ($v \sin i$) for AzV 327 (100 km s^{-1} , Bouret et al. in preparation). Although it could be an indication that the iron abundance in our targets is slightly smaller than the fiducial 0.2 Fe_{\odot} of SMC O-type stars, it could as well be related to a lower micro-turbulent velocity in their photospheres. Settling this issue requires quantitative modeling, which we will discuss later in this paper.

Let us now discuss IC1613-A13. As already said the N v resonance doublet (top panel of Fig. 2) is sensitive to the X-ray flux (not known for most of the stars here); it also often heavily blends with interstellar Ly α on the blue side of the profile, which is an additional issue for early-type O dwarfs as their wind terminal velocities are expectedly higher than for the late-type supergiants. Despite this, V_{∞} does appear to decrease with metallicity, a trend that is further confirmed on the other panels. Using the C IV $\lambda\lambda$ 1548, 1550 resonance doublet (third panel), we see that V_{∞} for the LMC star ($\approx 2700 \text{ km s}^{-1}$), intermediate between V_{∞} for the Galactic and SMC star. Remarkably, V_{∞} for IC1613-A13 and the counterparts in the SMC (MPG 324) are very similar, which might indicate that the metallicities in both galaxies are alike.

The conclusions are not as obvious for the mass-loss rate. For instance, the N v λ 1240 P Cygni profile in A13 is clearly as strong (both the absorption and emission components) as the profile in the Galactic star (HD 93205) and in any case stronger than in MPG 324 in the SMC. The second panel, showing O v λ 1371 seems to indicate that, the LMC star left aside, we do observe a trend for lower metallicity stars to have lower \dot{M} . The O v λ 1371 profile for IC1613-A13 is indeed almost completely photospheric while

Table 2. IDs, spectra and photometry for the comparison stars.

| Star | Comparison Stars - Sp. Type | Galaxy | FUV spectrum | V | B | E(B-V) ^a |
|------------|-----------------------------|--------|---------------------|-------|-------|---------------------|
| IC1613-A13 | | IC1613 | <i>COS</i> GO 12867 | | | |
| | HD 93205 - O3.5 V((f)) | MW | <i>IUE</i> SWP07959 | 7.76 | 7.76 | 0.28 |
| | LH81W28-5 - O4 V((f+)) | LMC | <i>STIS</i> GO 8633 | 13.92 | 13.74 | 0.15 |
| IC1613-B11 | MPG 324 - O4 V((f)) | SMC | <i>STIS</i> GO 7437 | 14.07 | 13.79 | 0.07 |
| | | IC1613 | <i>COS</i> GO 12867 | | | |
| | HD 76968 - O9.5 Ib | MW | <i>IUE</i> SWP20621 | 7.09 | 7.21 | 0.38 |
| WLM-A11 | BI170 - O9.7 I | LMC | <i>FOS</i> GO 5444 | 13.06 | 13.26 | 0.07 |
| | AzV 327 - O9.5II-Ibw | SMC | <i>STIS</i> GO 7437 | 13.25 | 13.47 | 0.04 |
| | | WLM | <i>COS</i> GO 12867 | | | |
| | HD 152424 - O9.7 Ia | MW | <i>IUE</i> SWP15021 | 6.31 | 6.71 | 0.66 |
| | BI170 - O9.7 I | LMC | <i>FOS</i> GO 5444 | 13.06 | 13.26 | 0.07 |
| | AzV 327 - O9.5II-Ibw | SMC | <i>STIS</i> GO 7437 | 13.25 | 13.47 | 0.04 |

^a Calculated from B-V (this table) and (B-V)₀ from (Martins & Plez 2006).

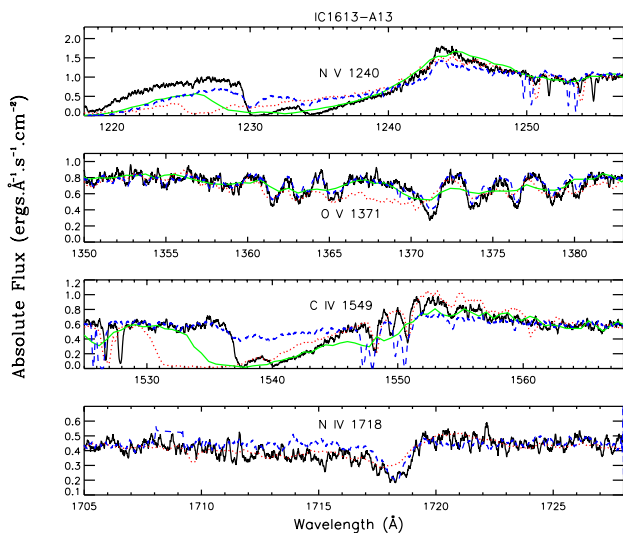


Figure 2. P Cygni profiles of A13 (in black). Overplotted in red, green and blue are the spectra of the Galactic, LMC and SMC stars (respectively) chosen for comparison (cf. Table 2). For plotting purpose, the fluxes were scaled by a factor 10^{14} .

the profile for MPG 324 (SMC) and HD 93250 (MW) present a blueward extension (stronger for the Galactic star). However, O V $\lambda 1371$ is one of the FUV line that is expected to be most sensitive to wind clumping (Bouret et al. 2005), together with N IV $\lambda 1718$. The later is shown in the bottom panel and the same comments hold for both lines (this wavelength range is not covered by the *STIS* spectrum of the LMC star). Care should be used when interpreting these profiles as their strengths also reflect the degree of wind clumping, that most likely varies from star to star. The gap in metallicity between our Galaxy and the SMC is large enough however, such that the weakening of the wind profile caused by the factor of five in metallicity is visible in this panel. Here again, the resolution of the LMC spectrum is too low to reach a firm conclusion about the strength of the O V $\lambda 1371$ profile relative to the SMC counterpart and IC1613-A13 accordingly.

The third panel, showing the C IV $\lambda\lambda 1548, 1550$ resonance doublet, further adds to the confusion. The expected qualitative trend is observed for the Galactic, LMC and SMC stars for the mass-loss rate (and terminal velocity). The absorption components of the P Cygni profiles for the three stars go from clearly satu-

rated (Galactic, then LMC) to unsaturated (SMC); the emission decreases in intensity as well. This is fully consistent with theoretical expectations from the radiatively-driven winds theory, but the behavior of IC1613-A13 is at odds with this predicted trend. Although its V_∞ seems quite similar to that of MPG 324 in the SMC, the intensity of its P Cygni profile is much stronger, suggesting that the mass-loss rate is higher. One should remember, however, that the intensity of the P Cygni profile is determined by $\dot{M} q_{C\text{IV}} A_C$ where $q_{C\text{IV}}$ is the ionization fraction of C IV and A_C the abundance of Carbon. Therefore, we cannot rule out that either the Carbon abundance or the C^{3+} ionization fraction, or a combination of both, is really lower in the SMC star such that the P Cygni profile is weaker. It is also noteworthy that the C IV P Cygni profile of IC1613-A13 shows well-defined narrow absorption components (NACs) that are useful to measure the wind terminal velocity (Prinja & Crowther 1998). DACs are also observed in several SMC O dwarfs of early spectral type (Bouret et al. 2013), where the absorption component is never saturated (see Fig. 2, the case of MPG 324).

To summarize this section, we find that the P Cygni profiles of IC 1613-B11 and WLM-A11 are compatible with the winds of these stars being weaker than winds of stars with similar spectral types and higher metallicity. Since Mokiem et al. (2007) showed that the wind quantities of massive stars in the Milky Way, the LMC and SMC follow a trend in quantitative agreement with the predictions of the radiatively-driven wind theory, it is tempting to conclude that the spectra of our targets also comply quantitatively with the theoretical expectations. The case of IC 1613-A13 is different and only ambiguous conclusions about the wind quantities and their dependence to metallicity is obtained from a qualitative comparison. We will now discuss the quantitative aspects of this conclusion, from the modeling perspective.

4 MODELS AND METHOD

For a more quantitative view of the wind properties, we compared the observed FUV + optical spectra of IC 1613-A13, IC 1613-B11 and WLM-A11 to synthetic spectra calculated with the NLTE stellar atmospheres code CMFGEN (Hillier & Miller 1998). CMFGEN computes NLTE line-blanketed model atmospheres, solving the radiative transfer and statistical equilibrium equations in the comoving frame of the fluid in a spherically-symmetric outflow. The models we computed account for the presence of the following species: H, He, C, N, O, Ne, Mg, Si, P, S, Cl, Ar, Ca, Fe, Ni, repre-

senting more than 7500 full levels (more than 2000 super-levels) and $\approx 135,000$ lines. The density structure is described as an hydrostatic part, in the quasi-static photospheric layers, smoothly connected to a β velocity law in the wind. The radiative acceleration is calculated from the solution of the level populations, and is used to compute a new inner structure (connected to the same β velocity law). The mass-loss rate, density, and velocity are related via the continuity equation. After convergence, a formal solution of the radiative transfer equation was computed in the observers frame (Busche & Hillier 2005), thus providing the synthetic spectrum for a comparison to observations.

We started from the stellar and wind parameters provided in Tramper et al. (2011) and tuned them as needed to get the best fit of the FUV and optical spectra together. The influence of clumping on the wind profiles was considered. Clumping is described in the framework of the optically-thin clumps formalism implemented in CMFGEN. The clumped wind density, $\rho(r)$, is related to the homogeneous (unclumped) wind density $\bar{\rho}$, and the volume filling factor f by $\rho(r) = \bar{\rho}/f$. The filling factor decreases exponentially with increasing radius (or, equivalently, with increasing velocity): $f = f_\infty + (1 - f_\infty) \exp(-v/v_{cl})$ where v_{cl} is the velocity at which clumping starts. More physical description of clumping exist nowadays and will be discussed in Sect. 8.2. A limitation of this parameterization is that f is monotonic whereas theoretical simulations by Runacres & Owocki (2002) and observational studies (Puls et al. 2006; Najarro et al. 2011) suggest it is non-monotonic. We found no need to tune v_{cl} to improve the fit to observed lines, hence we adopted a canonical $v_{cl} = 30 \text{ km s}^{-1}$ (Bouret et al. 2005).

The major consequence of this formalism is that mass-loss rates derived with clumped models are reduced by a factor $\sqrt{f_\infty}$, where f_∞ is the volume filling-factor associated with clumping, compared to mass-loss rates obtained from homogeneous models (e.g. Bouret et al. 2005). In the rest of the paper, we will refer to the ‘‘clumped’’ mass-loss rate (\dot{M} and f_∞ derived from the modeling of the FUV spectra) to compare to theoretical quantities and/or mass-loss rates from Tramper et al. (2014).

We also accounted for the effects of shock-generated X-ray emission in the model atmospheres. Since no measurements are available for IC 1613-A13, IC 1613-B11 and WLM-A11 in the X-ray wavelength range, we adopted the standard Galactic luminosity ratios $\log L_X/L_{bol} \approx -7$ (Sana et al. 2006), with the bolometric luminosity determined in the present study. We acknowledge however that there is no guarantee that this scaling ratio should prevail at low metallicity. Owocki et al. (2013) suggested for instance that this ratio should change with the physical nature of the shock generating the X-rays (radiative or adiabatic) and the wind density. Depending on the actual relation between the metallicity and the mass-loss rate, $\log L_X/L_{bol}$ could change accordingly.

4.1 Stellar and wind parameters

The photospheric (including surface abundances) and wind parameters have been derived following the same methodology as in previous papers (see e.g. Bouret et al. 2012, 2013).

- **Stellar luminosity:** The distance to IC 1613 and WLM were taken from Pietrzyński et al. (2006) and Urbaneja et al. (2008), respectively. We used the flux-calibrated *COS* spectrum, providing the flux distribution in the FUV wavelength range, together with optical photometry (cf. Table 2) to build spectral energy distribution (SED). The intrinsic stellar luminosity was then derived, by fitting

the SED. Note that we used the color excess quoted in Table 2 to take reddening into account, using the data by Cardelli et al. (1989).

- **Effective temperature and surface gravities:** T_{eff} was constrained from the helium (primarily He I $\lambda 4471$ to He II $\lambda 4542$ equivalent width ratio, as well as by fitting the line profiles) in the optical spectra. We add that the relative strength of helium lines was also used to constrain the helium abundance. Ratios of lines in the FUV spectra (Heap et al. 2006; Bouret et al. 2013, e.g.) were also used for further consistency, e.g. C IV $\lambda 1169$ to C III $\lambda 1176$, or N III $\lambda \lambda 1183-1185$ and N III $\lambda \lambda 1748-1752$ to N IV $\lambda 1718$ ratios. This is particularly important for the hottest star of the sample, namely A13, where the He I lines become weak (see also Rivero González et al. 2012, for the use of nitrogen optical lines to constrain T_{eff} for the earliest O-stars). The C IV $\lambda 1169$ to C III $\lambda 1176$ ratio is especially useful in early O-type stars because of its very good sensitivity to T_{eff} and weak dependance on gravity; hence we used it as the primary T_{eff} diagnostic in the UV.

The Stark-broadened wings of Balmer lines, especially H γ , were the primary constraint on $\log g$. The S/N of the *X-shooter* spectra is such that it is not possible to achieve a typical accuracy (1σ) better about 0.2 dex in $\log g$.

- **Microturbulence:** A constant microturbulent velocity of 15 km s^{-1} was adopted for calculating the atmospheric structure. To calculate the emerging spectrum, we used a radially dependent turbulent velocity (see also Hillier & Miller 1998). The microturbulence in the photosphere ξ_t was set mostly using the S V $\lambda 1502$ line, that is very sensitive to this parameter over a large range of T_{eff} . We further tuned it if necessary using the known sensitivity of some He lines to ξ_t (Villamariz & Herrero 2000; Hillier et al. 2003). In the outer region of the wind, the turbulence was adopted to fit the shape and slope of the blue side of the absorption component of the C IV 1548-1551 P Cygni profile.

- **Surface abundance :** The thousands of photospheric lines of iron ions (Fe III to Fe VI) present in the FUV are most useful to constrain the metal content of the stars. This shall provide an independent check of the stellar metallicity so far inferred from the ISM O/H ratio in the host galaxies of our targets. While the lines of Fe ions grow stronger with increased gravity and higher iron abundance and/or microturbulent velocity, the ratio of line strengths is most sensitive to temperature (see the discussion in Heap et al. 2006). Practically, we used T_{eff} , $\log g$, and ξ_t determined as we just presented to derive an iron abundance as reliable as possible. Abundances of α -elements included in the models (Ne, Mg, Si, S, Ni) were scaled down from the solar values of Asplund et al. (2005), adopting the same factor as for iron. Note that for the specific case of Si, we tuned the silicon abundance in the two late-type O supergiants, using several lines of Si III (triplet at $\lambda \lambda \lambda 1294.54, 1298.89, 1298.96$ or the singlets at $\lambda 1312.59$ and $\lambda 1417.24$) present in the *COS* spectra.

- *Carbon abundance:* C IV $\lambda 1169$, C III $\lambda 1176$ are prime indicators for carbon abundances. These lines proved to be sensitive to T_{eff} and ξ_t and C III $\lambda 1176$ further showed sensitivity to the wind density for the two stars with later spectral types. In this case, we gave more weight to C III $\lambda 1247$, which is clearly detected in IC1613-B11 and WLM-A11 and not affected by the adjacent, weak, N V resonance doublet.

The VLT/*X-shooter* spectra turned out to be quite noisy and with a spectral resolution somewhat too low, such that C III $\lambda \lambda 4068, 70$ were used only as secondary indicators for C/H determination for the late-type supergiants (B11 and A11). Besides, we did not include C III $\lambda \lambda \lambda 4647, 50, 51$ although is clearly detected in the spectra of B11 and A11. Martins & Hillier (2012) indeed showed

that it is very sensitive to the adopted atomic physics and other modeling assumptions³.

– *Nitrogen abundance*: In the UV, the photospheric lines N III $\lambda\lambda 1183$ -1185 and N III $\lambda\lambda 1748$ -1752 are used as primary diagnostics. N IV $\lambda 1718$ is also used for the late supergiants, but not for A13, as it is clearly affected by the stellar wind in this early-type star. In the optical N III $\lambda\lambda 4634$ -42 and N IV $\lambda 4058$ are the strongest nitrogen lines in the spectrum of A13, and were used as additional diagnostics for nitrogen abundance. Their formation processes, including their sensitivity to the background metallicity, nitrogen abundance, and wind-strength, have been discussed extensively by Rivero González et al. (2011, 2012).

– *Oxygen abundance*: The O IV $\lambda\lambda 1338$ -1343 lines usually serve as a diagnostic for O/H in the UV. Here however, they show a blue asymmetry that indicates a contribution from the wind for the earliest star (A13) with the stronger wind, and they are very weak (if detected at all) in the late-type supergiants. O III $\lambda\lambda 1150$, 1154 could be used instead but these lines are on the shortest side of the UV spectra and the flux level there is more uncertain. Similarly, O V $\lambda 1371$ is detected for the hottest star (A13) but it is very sensitive to the mass-loss rate and clumping parameters. Because the number of useful/reliable oxygen lines is so limited, the oxygen abundance was first set such that the sum of CNO is conserved, with respect to an initial mixture CNO scaled to the metallicity of the star. It was then tuned if necessary to improve the fit quality to O IV $\lambda\lambda 1338$, 1343.

• **Wind parameters**: The wind terminal velocities, V_∞ , were estimated from the blueward extension of the absorption component of FUV P Cygni profiles. Although the P Cygni profiles of the three targets are not saturated, narrow absorption components are visible, especially in N V and C IV profiles and were used to derive estimates of V_∞ , following the approach discussed in Prinja & Crowther (1998). The typical uncertainty in our determination of V_∞ is 100 km s⁻¹ (depending on the maximum microturbulent velocity we adopted).

Mass-loss rates were derived from the analysis of UV P Cygni profiles, such as C IV $\lambda\lambda 1548$, 1551, O V $\lambda 1371$ and N IV $\lambda 1718$ for A13 and Si IV $\lambda\lambda 1394$, 1403 and C IV $\lambda\lambda 1548$, 1551 for B11 and A11, respectively. We emphasize again the strong dependence of the N V resonance doublet on the adopted X-ray luminosity, especially for the stars with cooler T_{eff} . As $\log L_X/L_{\text{bol}}$ is not known for our targets, we did not use N V $\lambda 1238$, 1242 P Cygni profiles to constrain \dot{M} .

The β exponent of the wind velocity law was derived from fitting the shape of the P Cygni profile. The clumping parameters, f_∞ and v_{cl} were derived in the UV domain. We used O V $\lambda 1371$ and N IV $\lambda 1718$ (Bouret et al. 2005), as well as Si IV $\lambda\lambda 1394$, 1403 and C IV $\lambda\lambda 1548$, 1551. All these lines indeed present significant sensitivity to clumping in the temperature regime of our targets. Some photospheric lines in the optical presented some sensitivity to the adopted filling factor (and scaled \dot{M}). For photospheric H I and He lines, for instance, this is essentially caused by a wind contribution that is weaker in clumped models, which produces deeper absorption than smooth-wind models.

Synthetic spectra have been convolved with gaussian instrumental profiles, at the resolution delivered by HST/COS and VLT/X-

shooter, respectively. Then, we further convolved these spectra with a rotational profile to account for the projected rotational velocity of the star. For simplicity, we adopted the values listed Trammer et al. (2011) and checked on several FUV line profile for consistency (see e.g. Bouret et al. 2013). Given the moderate spectral resolving power and signal-to-noise ratio of the VLT/X-shooter spectra, we did not try to derive additional broadening mechanisms using the classical Fourier Transform method (Simón-Díaz 2010).

5 RESULTS OF THE MODELING

The best-fit of the FUV and optical spectra of the targets are presented in the Appendix, while the parameters of the corresponding model are listed in Table 3. We emphasize that the values we quote for \dot{M} in this table were obtained by fitting the FUV spectra we presented hereabove, but they do provide consistent fits to the optical spectra. For comparison to parameters derived from optical spectrum, we used the most recent work by Trammer et al. (2014) as the fitting procedure presented there was updated compared to Trammer et al. (2011) to account for the scaling of V_∞ with metallicity, and the qualitative conclusions already reached in Trammer et al. (2011) are unchanged.

5.1 IC 1613-A13

We find A13 to be cooler than in Trammer et al. (2014), although both T_{eff} overlap within the respective error bars. Since we used the ionization balance of C IV and C III as well as those of the iron ions present in the FUV to constrain the parameters, our T_{eff} estimate is therefore less prone to uncertainties related to the weakness of He I lines in the optical for such an early-type O star. We note that our value is very close to T_{eff} derived by Garcia et al. (2013) from the modeling with CMFGEN of a lower resolution COS spectrum of this star. The luminosity we derive, based on SED fitting, is a mere 0.09 dex smaller than in Trammer et al. (2014). On the other hand, we favor a surface gravity $\log g = 3.75$ over the lower value ($\log g = 3.65$ in Trammer et al. 2014), although the error bars are quite large in both case. This higher value stems mostly from the influence of $\log g$ on the global ionization balance (see Heap et al. 2006) and is also more compatible with the spectral/luminosity class of IC 1613-A13. As a consequence, the stellar, spectroscopic, mass we derive is in good agreement with the mass quoted by Trammer et al. (2014).

The helium fraction (by number) we derive is a factor of 2.5 times smaller than in Trammer et al. (2014). We find that such a high helium fraction as theirs would produce He II $\lambda 1640$ with a well-developed P Cygni profile, as well as strong wings in emission for the He II $\lambda 4686$ line (see Fig. 8). None of those are observed and we discarded this solution; it is also not consistent with the evolutionary status of this star.

The iron abundance, which we shall now refer to as the global metallicity, was first set at $\text{Fe}/\text{Fe}_\odot = 0.14$ (Trammer et al. 2011, and refs. therein). Models with an iron content typical of SMC ($\text{Fe}/\text{Fe}_\odot = 0.20$) and LMC ($\text{Fe}/\text{Fe}_\odot = 0.50$), as well as $\text{Fe}/\text{Fe}_\odot = 0.10$, were computed. The higher and lower metallicity options are easily discarded but on the other hand, it is not possible to rule out a SMC-like metallicity for IC 1613-A13. As already outlined in Sect. 4, the strength of the many Fe III to Fe VI lines (as well as S V $\lambda 1502$) depends on the adopted abundance as much as on the photospheric parameters T_{eff} , $\log g$ and the microturbulence ξ_t set in the spectrum calculation (cf. Fig. 3). Within error

³ We note however that the influence of Fe lines found by Martins & Hillier (2012) should be less than for galactic O stars because the iron (and more generally metal) abundance is expected to be down by a factor of five or more

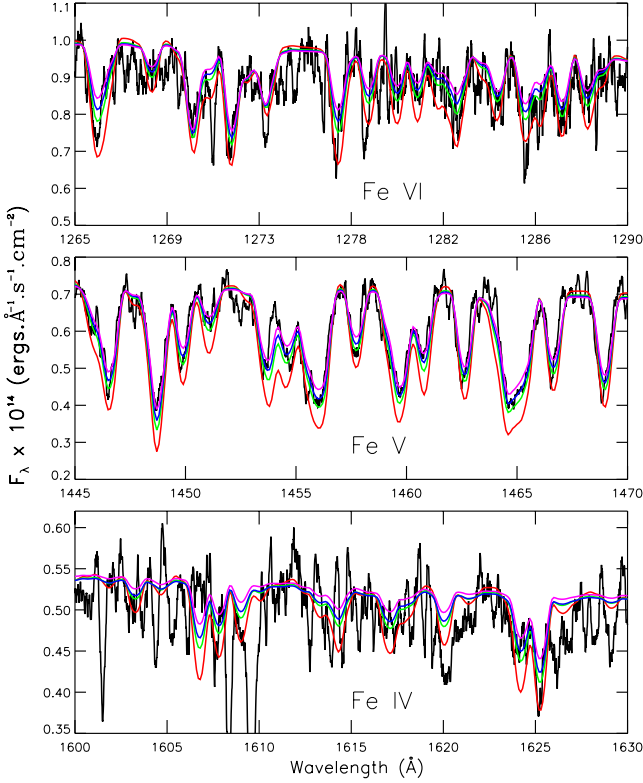


Figure 3. In black, line profiles for different transitions of iron ions (Fe VI to Fe IV from top to bottom) in the FUV range, observed for IC1613-A13. Overplotted in red, green, blue and pink are profiles obtained for models with the same parameters but the iron abundance, ranging to 1/2, 1/5, 1/7 and 1/10 Fe_\odot respectively.

bars of $\pm 5 \text{ km s}^{-1}$ for ξ_t , these lines are well fitted either adopting $\text{Fe}/\text{Fe}_\odot = 1/5$ or $\text{Fe}/\text{Fe}_\odot = 1/7$ for the iron content. The same conclusion holds for the Si IV resonance doublet and the S v $\lambda 1502$ line, which are purely photospheric in IC1613-A13.

An important conclusion of our study is that IC1613-A13 is carbon/oxygen-depleted and nitrogen-rich, compared to scaled-solar CNO abundances. The carbon abundance is very similar to the one we derived for MG 324, the SMC O4 V star we used for comparison in Fig. 2 (see also Bouret et al. 2013), but the nitrogen abundance is higher. The rotation rate of A13 is only mildly higher than in MPG 324 (we adopted $v \sin i = 98 \text{ km s}^{-1}$ for A13 as in Tramper et al. 2011, while $v \sin i = 70 \text{ km s}^{-1}$ for MPG 324). Furthermore, we note that IC 1613-A13 is more luminous and has lower surface gravity than MPG 324 (and other O4 V stars in the SMC for that matter), which points to a more advanced evolutionary status. An interpretation of the different abundances of these stars would require comparisons to predictions from evolutionary models, which is beyond the scope of this paper. In any case, the similar carbon abundance of IC 1613-A13 and MPG 324 implies that the observed difference in the C IV resonance profiles of these stars truly reflects a difference in mass-loss rates and wind clumping (T_{eff} is roughly the same for the two stars, hence the ionization fraction of C IV). The oxygen abundance conserving the sum of CNO, with respect to an initial CNO mixture that has the same scaling from the solar CNO mixture than the iron content of the model, produces a good fit to the FUV oxygen lines (O IV $\lambda\lambda 1338, 1342$ and O V $\lambda 1371$) and was adopted for the rest of this work.

The major modification with respect to Tramper et al. (2014)

Table 3. Stellar parameters derived from the spectroscopic analysis

| Properties | A13 | B11 | A11 |
|----------------------------------|-----------------|--------------------|--------------------|
| Spectral type | O3 V(f) | O9.5 I | O9.7 Ia |
| T_{eff} (K) | 42500. | 30000. | 29000. |
| $\log g$ (cgs) | 3.75 | 3.25 | 3.25 |
| $\log \frac{L}{L_\odot}$ | 5.62 | 5.45 | 5.69 |
| $M_{\text{spec}} [M_\odot]$ | $27.6 \pm 13.$ | $22.3 \pm 7.$ | $53.2 \pm 9.$ |
| ξ_t [km s^{-1}] | 25 | 15 | 10 |
| Y_{He} | 0.10 | 0.10 | 0.11 |
| ϵ_{C} | 7.00 ± 0.24 | 7.00 ± 0.30 | 7.00 ± 0.30 |
| ϵ_{N} | 7.78 ± 0.23 | 7.70 ± 0.20 | 7.70 ± 0.20 |
| ϵ_{O} | 7.90 ± 0.20 | 7.96 ± 0.30 | 7.96 ± 0.30 |
| $\text{Fe}/\text{Fe}_\odot$ | 0.2 | 0.2 | 0.2 |
| [C/H] (dex) ^a | -1.39 | -1.39 | -1.39 |
| [N/H] (dex) ^a | 0.00 | -0.08 | -0.08 |
| [O/H] (dex) ^a | -0.76 | -0.70 | -0.70 |
| f_∞ | 0.03 | 0.10 | 0.10 |
| V_∞ | 2180. | 1300. | 1400. |
| β | 0.8 | 1.0 | 1.0 |
| $\log(\dot{M}_{\text{FUV}})$ | -6.60 | -7.82 ^b | -7.95 ^b |
| $\log(\dot{M}_{\text{Tramper}})$ | -5.85 | -6.25 | -5.50 |
| $\log(\dot{M}_{\text{Vink}})$ | -6.07 | -6.51 | -6.41 |
| $\log(\dot{M}_{\text{Lucy}})$ | -6.82 | -7.65 | -7.54 |

Uncertainties on T_{eff} are $\pm 1000 \text{ K}$, ± 0.2 dex for $\log g$, ± 0.1 dex on $\log L/L_\odot$. As for the wind quantities, an uncertainty of ± 0.2 dex was estimated for the mass-loss rates (given in $M_\odot \text{ yr}^{-1}$), while V_∞ was measured within $\pm 100 \text{ km s}^{-1}$. For CNO abundances, $\epsilon_X = 12 + \log(X/H)$.

^a Defined as $[X/H] = \log(X/H) - \log(X/H)_\odot$. Solar values adopted from Asplund et al. (2005).

^b See Sect. 8.3 for a discussion about the true mass-loss rates from FUV

is about the wind parameters, that is the mass-loss rates, wind terminal velocities and clumping filling-factor, which we derive from the modeling of FUV P Cygni profiles. Fitting the COS spectrum of IC1613-A13 required a volume filling factor of $f_\infty = 0.03$. Aside from the well-known clumping diagnostics such as the O v $\lambda 1376$ and N IV $\lambda 1718$ lines, clumping turned out to be an important ingredient to fit the C IV $\lambda\lambda 1548, 1550$ P Cygni profile. This is because the ionization balance of carbon is shifted toward C^{4+} throughout the wind, at the effective temperature of IC1613-A13 and clumping helps C^{4+} recombine to C^{3+} . More generally, this is true for T_{eff} in the range usually covered by O4 dwarfs and earlier (typically $T_{\text{eff}} \geq 42,000 \text{ K}$). For T_{eff} as high as quoted in Tramper et al. (2014), the ionization fraction of C^{4+} is actually close to unity and the resonance doublet is weak for an homogeneous wind. Significant level of clumping is required to produce enough C^{3+} such that a strong C IV $\lambda\lambda 1548, 1550$ P Cygni profile forms again. This dependence of the C IV profile on the clumping volume filling factor might explain why its more difficult to see the trend of \dot{M} with metallicity in A13 than in the late-type supergiants (cf. Sect 3).

The clumped mass-loss rate is $2.5 \times 10^{-7} M_\odot \text{ yr}^{-1}$, while the wind acceleration is $\beta = 0.8$ and the wind terminal velocity is 2180 km s^{-1} . The later are in excellent agreement with the values derived by Garcia et al. (2014) from the modeling of low resolution COS spectrum of this star, with the SEI method (Sobolev with Exact Integration, Hamann 1981; Lamers et al. 1987).

5.2 IC 1613-B11 and WLM-A11

The photospheric parameters derived for IC 1613-B11 and WLM-A11 from the analysis of their FUV + optical spectra are consistent with their spectral classification, and in relatively good agreement with those of Tramper et al. (2014). The surface gravity we derive for IC 1613-B11 is actually more consistent with $\log g$ derived by Bresolin et al. (2007). We note that the Si III lines ($\lambda\lambda 1295 - 1299$) get weaker as $\log g$ decreases. They argue against $\log g \leq 3.2$, which we adopted as a lower limit as it provides the best fit to the FUV spectrum while still maintaining a very good agreement with the optical spectrum. The uncertainty on $\log g$ from the optical analysis alone is quite large because of the modest signal-to-noise ratio of the *X-shooter* spectra. Using the FUV spectra in this case does help better constrain the value of the surface gravity.

We also note that, including error bars, WLM-A11 is over-luminous (by $\approx 0.2 - 0.3$ dex), compared to luminosity class I stars with similar spectral type in the SMC or LMC (see e.g. Massey et al. 2009). This trend is also present, although even stronger, in Tramper et al. (2011, 2014), and is consistent with the “a” subscript on its classification.

For the photospheric parameters listed in Table 3, the iron lines in the FUV spectra of IC 1613-B11 and WLM-A11 are well reproduced with models having $\text{Fe}/\text{Fe}_\odot = 0.14$ and $\xi_t = 17 \text{ km s}^{-1}$ and 13 km s^{-1} , respectively. However, minor changes to the micro-turbulence in the models (a decrease by 3 km s^{-1}) to increase Fe/H to SMC-like value provides as good a fit as well. Figure 4 illustrates the impact of such a minor variation of ξ_t on the profiles of Fe IV and Fe V photospheric lines. Although the SNR of the *COS* spectra do not allow to rule out the lower metallicity ($\text{Fe}/\text{Fe}_\odot = 0.14$) option, we found that a SMC-like silicon abundance is more supported by the lines of Si III (see Sect. 4) present in these late-type O supergiants. The synthetic spectra of IC 1613-B11 and WLM-A11 presented in the Appendix were obtained with models having an iron content $\text{Fe}/\text{Fe}_\odot = 0.2$, which we adopted as the metallicity of IC1613-B11 and WLM-A11.

As expected from their evolved status, the surface abundances of IC 1613-B11 and WLM-A11 present signs of CN processing. Carbon is depleted while we measured nitrogen enhancement with respect to the adopted baseline values for the metallicities of IC 1613 and WLM. On the other hand, the scarcity of sensitive diagnostics for oxygen abundance in the FUV makes its measure questionable for these two stars. In the optical, several lines of O II are present, in principle, but are very weak and are not useful given the moderate signal-to-noise ratios of the *X-shooter* spectra. We checked that a simple scaling to 0.2 the solar oxygen content gives the best agreement with the observed spectra however. With this scaling, the sum of CNO scaled to 0.2 (as for the SMC) its solar value is also roughly conserved. Finally, we find that helium is slightly enriched in WLM-A11, while no change to He/H is needed to reproduce He line strengths in IC1613-B11.

Here again, the most salient discrepancies with the study by Tramper et al. (2014) are the wind parameters. The high mass-loss rates they derived are firmly ruled out, producing much stronger P Cygni profiles than observed (cf. Fig. 5). In our modeling, the (clumped) mass-loss rates are $1.5 \times 10^{-8} M_\odot \text{ yr}^{-1}$ and $1.1 \times 10^{-8} M_\odot \text{ yr}^{-1}$ for IC 1613-B11 and WLM-A11, respectively.

With these models, we could obtain a reasonable agreement with the observed P Cygni profile of C IV resonance doublet, the Si IV resonance doublet as well as N V $\lambda\lambda 1238, 1242$, although none of our models could fit these three profiles with the same level of quality simultaneously. The case of IC1613-B11 is the most

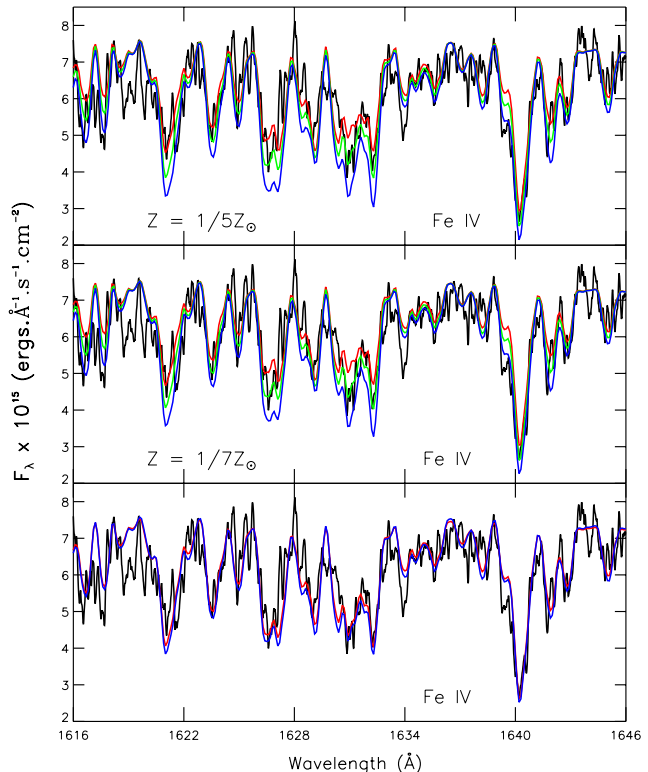


Figure 4. In black, a portion of observed spectrum of WLM-A11 showing several lines of Fe IV around He II $\lambda 1640$. The sensitivity of the Fe IV lines to the micro-turbulence is shown, for models having $\xi_t = 7 \text{ km s}^{-1}$ (red), 10 km s^{-1} (green) and 12 km s^{-1} (blue). The top panel presents models computed with $\text{Fe}/\text{Fe}_\odot = 0.2$ (SMC-like), the models in the center panel have $\text{Fe}/\text{Fe}_\odot = 0.14$. The bottom panel shows a models with $\text{Fe}/\text{Fe}_\odot = 0.2$ and $\xi_t = 10 \text{ km s}^{-1}$ (red), and a model with $\text{Fe}/\text{Fe}_\odot = 0.14$ and $\xi_t = 13 \text{ km s}^{-1}$ (blue).

problematic as we could never reach an excellent fit of the C IV profile for this star with our models. At low velocities, the absorption component of the observed P Cygni profile is stronger than predicted by the models, unless we increase \dot{M} to such extent that in the synthetic profile, the absorption is too strong near V_∞ and we also produce a strong emission component that is not observed in C IV. Note that this behavior is typical of late-type O dwarfs exhibiting the “weak-wind” problem, although IC 1613-B11 is above the luminosity threshold usually found for these stars ($\log L/L_\odot \approx 5.2$, e.g. Martins et al. 2005; Marcolino et al. 2009). Furthermore, a well-defined P Cygni profile is produced for the Si IV doublet, also not observed.

The P Cygni profiles, although relatively weak, presented good sensitivity to variations of the clumping filling-factor. The filling factor is moderate in both cases, that is $f_\infty = 0.1$, implying a reduction of a factor of three for \dot{M} compared to an homogeneous case. The \dot{M} we derive correspond to a regime where H α is mostly insensitive to constrain mass-loss rates (Marcolino et al. 2009). The modeling of the FUV and optical spectrum of supergiant stars in the SMC (Bouret et al., in preparation) yields mass-loss rates in good qualitative and quantitative consistency with those derived here for IC 1613-B11 and WLM-A11. The mass-loss rate derived for AzV 327, for instance, is roughly three times as high as those of IC 1613-B11 and WLM-A11, a trend that is anticipated from the relative strength of their P Cygni profiles (cf. Fig. 1).

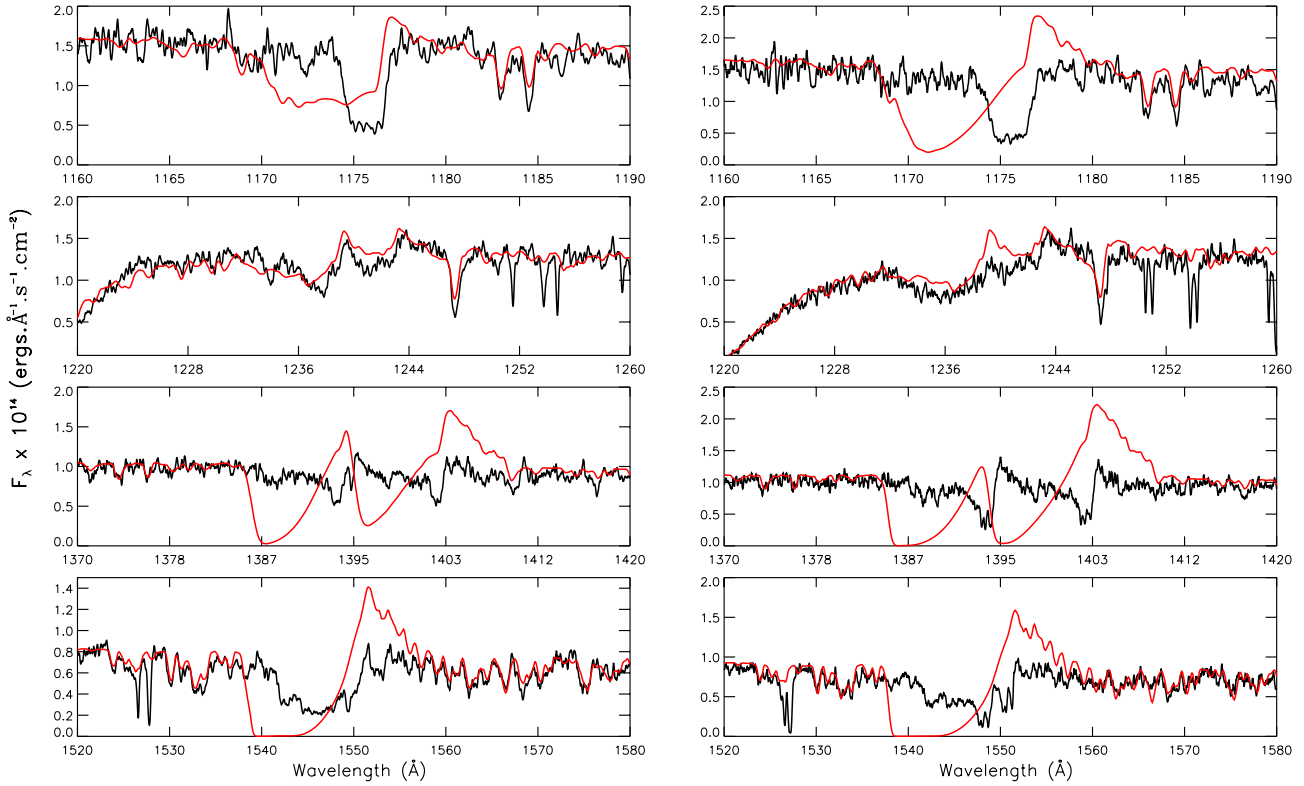


Figure 5. In black, line profiles for different transitions in the FUV range, observed for IC1613-B11 (left) and WLM-A11(right). Overplotted in red, P Cygni profiles produced by models using the parameters from Tramper et al. (2014).

The exponent of the velocity law was constrained from the weak emission component of the P-Cygni profile. Its value is consistent with theoretical predictions (Mujeres et al. 2012), but is lower than found by Mokiem et al. (2006) or Massey et al. (2009) for late-type supergiants. Furthermore, the wind terminal velocities are consistent with V_∞ measured by Massey et al. (2009) from UV data for late-type supergiants in the Magellanic Clouds. However, we stress that the P Cygni profiles in B11 and A11 are weak enough that the wind terminal velocities are rather difficult to measure. Most particularly, several lines of Fe IV overlap the blue edge of the C IV resonance doublet P Cygni profiles. These lines were not an issue for IC 1613-A13 but they are stronger at the lower T_{eff} of B11 and A11. With $\Delta V \approx 1200 \text{ km s}^{-1}$, they fall right in the typical range for V_∞ indicated for B11 and A11 by the discrete absorption components, following Prinja (1998). Although the CMFGEN models do account for these Fe IV lines, their sensitivity to T_{eff} , the adopted Fe/H, the microturbulence and even $\log g$ could introduce an additional uncertainty in the determination of V_∞ , with expected repercussions on the predicted mass-loss rates (see Sect. 10).

6 METALLICITY OF THE MASSIVE STARS OF IC 1613 AND WLM

The striking conclusion by Tramper et al. (2011) of a discrepancy between observed and predicted mass-loss rates relied for a large part on the adopted metallicities for IC 1613, WLM and NGC 3109. The (low) metal content for these galaxies has been measured by various techniques, which all point towards a SMC-type metallicity or even below. In their more recent work, Tramper et al. (2014)

acknowledged that the metallicities they considered in their initial study were likely underestimated. In the present study, we have a direct access to the global metallicity of the stars through thousands of photospheric lines of iron ions (Fe III to Fe VI) present in the FUV spectral range. Oxygen abundance diagnostic is also available (cf. Sect. 4.1). Before comparing empirical mass-loss rates as derived from the modeling of FUV spectra to theoretical ones, we first need to discuss how the metal content we derived compares to previous determinations.

6.1 Oxygen

As discussed in Sect. 5.1 and 5.2, the oxygen abundance is difficult to constrain accurately in the three stars. The best we can say at this point is that oxygen abundances such that the total CNO is conserved do provide good fits to the scarce diagnostics available. In principle, the evolved status of IC1613-B11 and WLM-A11 should translate into oxygen depletion, compared to the initial CNO mixture. Although we do not need such a depletion to reproduce the O IV lines present in the FUV spectra of both stars, we cannot rule out that oxygen abundances are actually lower. Only for IC 1613-A13 does such a depleted oxygen content manifest itself (maybe a consequence of the earlier spectral type, hence higher mass, implying faster evolution), but is however moderate. In summary, O/H in the three stars ranges between 1/7 – 1/5 the solar oxygen content, but we emphasize again that these estimates are poorly constrained and may be revised provided stronger diagnostics become available. How relevant these abundances are when dealing with comparisons between observed and predicted mass-loss rates of massive stars is however questionable.

6.2 Stellar Iron Content

Although the low oxygen (and more generally α -elements) content of IC 1613 and WLM is confirmed from FUV spectroscopy, direct measures of the iron abundance are more relevant to study the metallicity dependence of mass-loss. It is expected that the mass-loss rates of massive stars are determined by the radiative acceleration below the sonic/critical point in the wind, which is predicted to be driven by the iron group elements for O-type stars in the metallicity regime of our sample (Vink et al. 2001). Therefore, such measures of the iron abundance as those we achieve in this work are mandatory to compare empirical mass-loss rates to theoretical predictions, and in any case are more relevant than metallicities based on α -elements abundances. Iron abundance determination of course relies on the strength of iron lines which depends on the actual iron ionization. The later depends on the effective temperature and gravity (e.g. Heap et al. 2006). For a given temperature, the ionization is higher at lower gravities as expected from the Saha equation and the numerous iron lines grow stronger. Iron lines may also look stronger because of higher microturbulence ξ_t , as shown in Hillier et al. (2003) and Bouret et al. (2003). This degeneracy of the ionization balance of iron with the photospheric parameters is such that deriving the iron abundance from fits to the iron forest requires T_{eff} , $\log g$ and ξ_t to be determined from other diagnostics, which we have at our disposal through the analysis of the optical spectra for instance. From the joint analysis of the FUV and optical data, we found that for the three stars presented here, $[\text{Fe}/\text{H}] = -0.66$, i.e. their iron content is SMC-like.

In IC 1613, stellar iron abundances of $[\text{Fe}/\text{H}] = -0.67$ have been inferred from spectroscopy but for late-type, evolved stars (e.g. M type supergiants Tautvaišienė et al. 2007). Alternatively, photometric studies were performed to measure the iron to hydrogen ratio of stars on the red giant branch (Cole et al. 1999; Skillman et al. 2003; Minniti & Zijlstra 1997; McConnachie et al. 2005). These measures, however, determine the iron content of an older stellar population, while the objects we are dealing with here belong to a young stellar population. To our knowledge, no other measures exist of the present-day iron abundance as probed here through high spectral-resolution FUV spectroscopy and quantitative analysis of the forest of iron lines. The iron content we derive for the two stars in IC 1613 is also compatible with the study of the star formation history of IC 1613 by Skillman et al. (2003); these authors indeed found that the metallicity increased from $[\text{Fe}/\text{H}] = -1.3$ to -0.7 over the age of the galaxy. It is also noteworthy that using oxygen + silicon abundances as a proxy for the global abundance of α -elements, $[\alpha/\text{Fe}]$ is solar in our case (or slightly lower for IC 1613-A13). Given the uncertainties in both the abundances for α -elements as well as iron, this is however in qualitative agreement with the conclusions of Tautvaišienė et al. (2007) for IC 1613. Finally, we note that from a qualitative comparison of FUV spectra of OB stars in IC 1613 with OB stars in the SMC, Garcia et al. (2014) also argued that the iron contents are similar in both galaxies.

On the other hand, Urbaneja et al. (2008) quote a (present-day) metallicity of $\log(Z/Z_{\odot}) = -0.8 (\pm 0.2)$ for WLM-A11, although it is not derived from the direct analysis of iron-group lines. Although this value for Z/Z_{\odot} agrees with our estimate of the metallicity within the error bars, the average metallicity of the A and B supergiants analyzed by Urbaneja et al. (2008) is $\log(Z/Z_{\odot}) = -0.87 (\pm 0.06)$. This lower value is not favored by the spectroscopic analysis in our case, although better signal-to-noise ratio of the spectrum of WLM-A11 would be required to firmly discard this solution. We note that the metallicity of A-supergiants analyzed in

WLM by Venn et al. (2003) is however even higher than ours (with $[\text{Fe}/\text{H}] = -0.38 \pm 0.20$). The ranges in $[\text{Fe}/\text{H}]$ are large enough that despite measure uncertainties, they hint to a real scatter in the star-to-star metal content in WLM. This comes as a surprise as WLM-A11 and the stars analyzed in Venn et al. (2003) are located within the same region of the WLM galaxy.

Overall, our joint analysis of the FUV and optical spectra reveals that the iron content of the three stars is similar to the SMC. In this sense, the theoretical mass-loss rates are expected to be higher than previously considered, although by a fairly limited factor of ≈ 1.3 . This is far from being enough to account for the strong discrepancy discovered by Tramper et al. (2011) and confirmed in Tramper et al. (2014), especially for the late supergiants. The wind terminal velocities are also impacted by the metallicity, although to lesser extent, which does not change this conclusion.

7 BINARY STATUS

Multiplicity can impact the mass-loss determination in several way (see the discussion in Tramper et al. 2011). The issue of multiplicity among massive stars has become very important in the past few years, with results for galactic massive stars pointing to fractions of stars with companions ranging from 75% (Mason et al. 2009, for clusters and associations in this specific case) and up to a striking 91% (Sana et al. 2014). At lower metallicity, results obtained within the VLT-FLAMES Tarantula Survey (Sana et al. 2012, and refs therein), point to a fraction of more than 50% binaries within the sample, once corrected for observational biases.

Concerning IC 1613-A13, the SED fitting is compatible with the star being single; the fluxes from the *COS* spectrum and the photometry (cf. Table 2) are well accounted for by the SED produced by a single-star model as computed with CMFGEN. The luminosity we derive is slightly higher (within 0.2dex) than those we obtained for (three) stars with close spectral type and effective temperature in the SMC (Bouret et al. 2013). However, one of these stars, namely MPG 324 that we used for morphological comparison in Sect. 3 (see also Table 3 and Fig. 2) is probably a single-lined binary as indicated from small radial-velocity variations (Evans et al. 2006), even though its theoretical SED from CMFGEN is compatible with the observed one. The case of MPG 324 suggests that we cannot firmly rule out the presence of a companion for IC 1613-A13 from the SED fitting approach only. Nevertheless, we can safely conclude that since the putative companion is of low mass enough that it does not show up in the observational SED, it is unlikely to impact the wind signatures we observe in the FUV spectrum.

The effective temperature, surface gravity and luminosity of IC 1613-B11 are compatible with those derived for stars with same spectral type/luminosity class in the MCs (e.g. Massey et al. 2009), for which no signs of multiplicity are known. Much like for IC 1613-A13, we do not see an influence from a potential companion on the SED of IC 1613-B11; here again, if the star is in a binary system, it must be with a companions of late type, whose luminosities must be low, hence, expectedly, the mass-loss rate. More significantly, the photospheric parameters of IC 1613-B11 are consistent within the error bars, with the calibration in Martins et al. (2005) for an O9.5 supergiant. Although low metallicity stars are known to be on average hotter and more luminous than their galactic counterparts for a given spectral, it is well-known that these differences decrease at later spectral type and practically vanishes by B0 (see e.g. Table 9 in Massey et al. 2005). The spectroscopic mass is also

consistent with this calibration, which further supports the single star interpretation.

The case of WLM-A11 is somewhat different. The SED fitting indicates that this star is more luminous than a normal O9.7 supergiant (also denoted by the "a" subscript of its spectral classification). The photospheric radius we derive and the surface gravity we measure are such that the star is then roughly twice as massive as other late-type supergiants of similar spectral properties, including IC 1613-B11 or stars in Massey et al. (2009). Such a high spectroscopic mass ($\geq 53 M_{\odot}$) is actually more characteristic of O-supergiants with early spectral types (e.g. Massey et al. 2009; Bouret et al. 2012). This might indicate that WLM-A11 is actually in a binary system or that there is an unresolved star in the foreground, contributing to the observed fluxes. We will come back on the influence of changing the stellar luminosity on mass-loss prediction, in a following section.

8 FUV MASS-LOSS RATES AND UNCERTAINTIES

Tramper et al. (2011, 2014) relied on the fitting of the $H\alpha$ (and He II $\lambda 4686$ line for the hotter objects) to measure the mass-loss of their targets. Known advantages are an easy and robust abundance determination and ionisation balance calculation. The sensitivity of $H\alpha$ is limited to stronger winds however, showing only moderate line core filling for mass loss rates between 10^{-6} and $10^{-7} M_{\odot} \text{ yr}^{-1}$ (see Fig. 5. in Marcolino et al. 2009). Because of their low metallicity, our targets should have mass loss rates in this parameter range (Vink et al. 2001). Detailed investigations should therefore rely on diagnostics showing sensitivity in this regime, namely FUV. Obviously, mass loss determinations in this spectral range also suffer from specific uncertainties related to the assumptions adopted in the modeling.

8.1 Abundances, Ionization and Wind Acceleration

The observed *COS* spectra present three important lines of carbon ions, namely C IV $\lambda 1169$, C III $\lambda 1176$ and C III $\lambda 1247$, that we used to measure the photospheric abundance of carbon. Within the uncertainties on C/H, the mass-loss rates of the targets could vary by at most a factor of two (but see below for a comment on the influence of \dot{M} on the C III $\lambda 1176$ line in the late-type supergiants). We emphasize that the predicted (wind) profiles of the Si IV resonance doublet are reasonably reproduced in our models of the late supergiants (cf. Fig. A3 and Fig A5). The Si element does not suffer, a priori, from the uncertainties related to carbon, as it is not involved in nuclear burning until very much later phases of the evolution of massive stars. Changing \dot{M} by a factor of two (i.e. within the boundaries of the relative uncertainty due to the carbon abundance) would change the profiles of Si IV resonance doublet enough that we can rule out these solutions.

The other obvious uncertainty is related to the ionization fraction of CNO ions. This might be a potential flaw of the FUV-based mass-loss determination, compared to hydrogen-helium based methods for photosphere + wind properties determination. This is because of uncertainties in the predicted flux levels at $200 \leq \lambda \leq 400 \text{ \AA}$, or more exactly differences in the flux levels predicted by state-of-the-art NLTE, line-blanketed models for massive stars (Puls et al. 2005). These differences translate in differences in the predicted populations of important ions such as C IV or N V for instance, hence on the estimate of the mass-loss rate.

Puls et al. (2005) emphasized that the uncertainties on the flux levels mostly impact the ionization fractions in the outer part of the winds, where they translates into differences in population of typically ± 0.15 dex, while they agree almost perfectly everywhere else. In our case, we are able to reproduce line ratios of different ionization stages of carbon, nitrogen, and oxygen which should guarantee that the flux slope in the critical range $200 \leq \lambda \leq 400 \text{ \AA}$ is correct. In any case, the ionization fraction of carbon, nitrogen and silicon ions should be accurate within a factor of a two, which does not change our conclusion on the actual mass-loss rates of our targets.

We can obtain a good grip on the wind velocity law, acceleration parameter and terminal velocity, from fitting of the slope of the emission component of the P Cygni profiles. It is in any case more robust than what can be done from optical lines alone when the line profiles are in absorption, in which case these parameters are not accessible thus increasing the uncertainty in the derived mass-loss rate, by a factor from 2 to 3 (Puls et al. 1996). In our case, the uncertainty in β and V_{∞} reflects in a moderate correction on \dot{M} only, which again does not change the conclusion of the present paper. Note that uncertainties on V_{∞} have an influence when dealing with the modified wind-momentum-luminosity relation (see e.g. Kudritzki & Puls 2000). The values of V_{∞} we measure are for instance $\approx 25\%$ different from those listed in Tramper et al. (2014), higher for IC1613-A13, but smaller for IC1613-B11 and WLM-A11.

8.2 Clumping

Wind clumping and the formalism used to describe it, is another important issue for the determination of mass-loss rates. It modifies the predicted line profiles for a given \dot{M} and this parameter cannot be considered separately of clumping parameters anymore.

Clumping as implemented in CMFGEN is usually referred to as micro-clumping (Hillier & Miller 1999, and refs therein). Its influence on \dot{M} determinations in O stars, both from FUV and optical diagnostics has been tested and discussed extensively for stars in the Galaxy and the SMC (e.g. Hillier et al. 2003; Bouret et al. 2005, 2012, 2013). The volume filling factors (f_{∞}) associated with the clumped models for our three targets ($f_{\infty} = 0.03$ for IC16-A13, and $f_{\infty} = 0.1$ for IC1613-B11 and WLM-A11) are in line with those found in these studies. They imply that the mass-loss rates are scaled down by factors 6 and 3 (respectively), compared to the homogeneous values that would be derived from fitting $H\alpha$. Note that with the adopted parameterization of clumping in CMFGEN (see Sect. 4), the volume filling factor in the formation region for the $H\alpha$ line is much higher than the value f_{∞} .

However, the filling factor approach is admittedly too simple. It considers optically thin clumps, an assumption valid for the continuum but not so much for the lines. Furthermore, it does not account for the interclump medium which is important for producing the P Cygni profiles of super ionized species (Zsargó et al. 2008) or, even more fundamentally, because void interclump medium is physically unlikely (e.g. Owocki et al. 1988; Šurlan et al. 2013; Sundqvist et al. 2014). It also ignores porosity, both in spatial and in velocity space (e.g. Oskinova et al. 2007; Sundqvist et al. 2011). A detailed study by Sundqvist et al. (2014) concluded that velocity-porosity, *a.k.a vorosity*, impacts both the line profiles (diagnostics) and mass-loss properties (dynamics), in contradiction with an earlier result by Šurlan et al. (2013) and based on a different approach, showing that spatial porosity was most important.

Notwithstanding the very different levels of physical sophisti-

cation to describe the nature of wind clumping and its effects (e.g. the role of porosity/vorosity), studies have found that the corrections to mass-loss with respect to theoretical predictions (the widely used recipe by Vink et al. 2001) should be less than a factor of 1.5 – 2.5 typically (Bouret et al. 2012; Šurlan et al. 2013; Sundqvist et al. 2014). This difference is actually very reasonable given the uncertainties related to both approaches, namely NLTE radiative transfer codes used to describe clumped stellar winds on one hand, and Monte-Carlo calculations of the radiative force used to predict mass-loss rates on the other hand.

Although these results were obtained for the same early-type Galactic supergiants with fairly dense winds, it is tempting to argue that the mass-loss rate we obtained, at least for IC1613-A13 which has a relatively dense wind, is realistic within the same margin, enough to provide a robust comparison basis against theoretical predictions.

8.3 Line force, momentum equation and implications

Whatever the physical nature of clumping, the presence of inhomogeneities in the wind makes it very difficult to determine the systematic errors associated with our mass-loss rates estimates. This is dictated by the lack of diagnostics, a problem exacerbated in stars that have weaker winds. Typically in the FUV we only have a few lines suitable for mass-loss determinations, and these line often have other sensitivities. For example in A13, the only wind diagnostics are the C IV and N V doublets, N IV $\lambda 1718$, and the absence of O V $\lambda 1371$, while in A11 we lose O V as a diagnostic but gain the Si IV doublet. For an inhomogeneous wind we have multiple parameters that describe the clumping, porosity, and porosity in velocity space that need to be determined.

In our modeling we have adopted the volume filling factor approach which has only two free-parameters, and one of which (the location at which clumping starts) is not well constrained. However, we have one additional consistency check that can be utilized. While CMFGEN does not compute the mass-loss rate self consistently, it does compute the radiative force, hence we can check how well the momentum equation is satisfied.

For A13 we find that the momentum equation is not satisfied – we deposit too much momentum in most of the wind, and this inconsistency cannot be changed by altering the velocity law while remaining constant with the observations⁴. Three possible solutions to the inconsistency are:

(i) An incorrect ionization structure.

(ii) Additional hot gas that we are not detecting. In the standard wind-driven wind model, it is assumed that hot shocked gas, arising from the radiation driven wind instability, rapidly cools. While this is likely to be valid for the wind of a star like ζ Pup (see, e.g., discussion by Hillier et al. 1993), the assumption will eventually become invalid as the density declines (Drew et al. 1994; Martins et al. 2005; Lucy 2012). Recently Huenemoerder et al. (2012) showed that the X-ray emission from μ Columbae originated in the

⁴ We ignore issues in accelerating the wind around the sonic point. In general we have too little line force at, and just above, the sonic point to accelerate the flow. Much of this discrepancy arises from issues with the choice of the microturbulent velocity: driving a stationary wind through the sonic point requires the microturbulent velocity to be much less than the sound speed. Although this is typical for O supergiants, it is not the case here – the microturbulent velocity is of order 0.5 times the sound speed.

wind, and required a hot gas component with a mass-loss rate in excess of that inferred from analysis of UV lines.

(iii) We are underestimating the mass-loss rate due to the effects of porosity and/or vorosity.

We dismiss the first one since in CMFGEN the predicted and observed ionization are consistent (see comments above). For A13 we also argue that in its relatively dense wind, the hot gas component is probably not important. However, consistent with other findings, porosity and vorosity could be important. If we adopt the same f_∞ and $\dot{M} = 5.5 \times 10^{-7} M_\odot \text{ yr}^{-1}$ we find much better agreement with the radiation force and that required to drive the wind. However, absorption features in the spectrum are now too strong. For $f_\infty = 0.1$ and $\dot{M} = 4.0 \times 10^{-7} M_\odot \text{ yr}^{-1}$ the situation is somewhat more intermediate – we somewhat deposit too much momentum between 100 and 1600 km s^{-1} , and somewhat too little in the outermost regions ($V > 2000 \text{ km s}^{-1}$).

Thus for A13 we conclude that our derived mass-loss rate is underestimated, at most, by a factor of two. This is consistent with our finding in ζ Pup where we found $\dot{M} = 2.0 \times 10^{-6} M_\odot \text{ yr}^{-1}$ for $f_\infty = 0.05$ using multiple diagnostics. However we could only fit the P V resonance doublet with an abundance a factor of two less than solar. If we assume the solar abundance is applicable, this would imply that vorosity/porosity effects influence mass-loss rates derived from the P V doublet by about a factor of two.

For A11 and B11, with much weaker winds, the situation is much more problematical. Let us discuss the case of A11 as an example. The mass-loss rate of $1.1 \times 10^{-8} M_\odot \text{ yr}^{-1}$ is a factor of three less than the limit for a single optically thick line located at the emission peak of the SED (L/c^2). This inconsistency is borne out when one examines the momentum equation – the radiation force that we derive is typically a factor of 5 to 10 times larger than that required to drive the flow. This discrepancy indicates that some fundamental assumption in our modeling is incorrect.

For A11 we believe that the problem is twofold. In its weak wind it is possible that the gas does not cool after it is shocked. Thus a significant fraction of the wind is in hot gas – a result consistent with the use of X-ray filling factors near unity in order to get a $\log L_X/L_{\text{bol}} \approx -7$. The second is that in these weaker winds, the influence of porosity/vorosity is more important. An alternative is that wind dynamics is influenced by the presence of a strong magnetic field but since the issue of weak winds is persistent, even in stars where a magnetic field is not detected (e.g., 10 Lac, David-Uraz et al. 2014), this cannot be the answer. If we adopt $f_\infty = 0.1$ and $\dot{M} = 3 \times 10^{-7} M_\odot \text{ yr}^{-1}$, there is reasonable consistency between the radiative force and that required to drive the flow. Of course this mass-loss rate produces a spectrum very inconsistent with that observed.

Independent of the cause of the discrepancy, we might expect our assumptions to be more valid deeper in the wind. Thus we decided to consider a model in which we varied the mass-loss rate as a function of the radius r , thus mimicking a wind in which, for example, a lot of the gas becomes hot and does not contribute to the observed UV spectrum. In the test case we assumed $\dot{M} = 7.7 \times 10^{-8} M_\odot \text{ yr}^{-1}$ in the inner wind, and $1.1 \times 10^{-8} M_\odot \text{ yr}^{-1}$ in the outer wind, with a smooth transition between them. With this model two distinct features were revealed:

(i) The higher mass-loss-rate model desaturates the C III triplet line near 1176 Å, and produces a weak blue wing. The profile is in better agreement with observations, than our best fit model.

(ii) The higher mass-loss-rate model produces a slight blueshift,

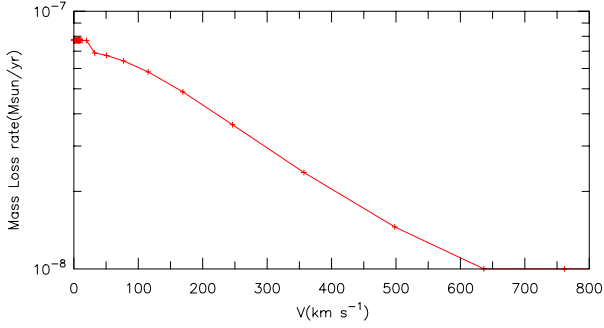


Figure 6. Variation of the mass-loss rate, plotted here as a function of the velocity in the wind. The model was used to compute the spectrum presented in Fig. 7 (blue line).

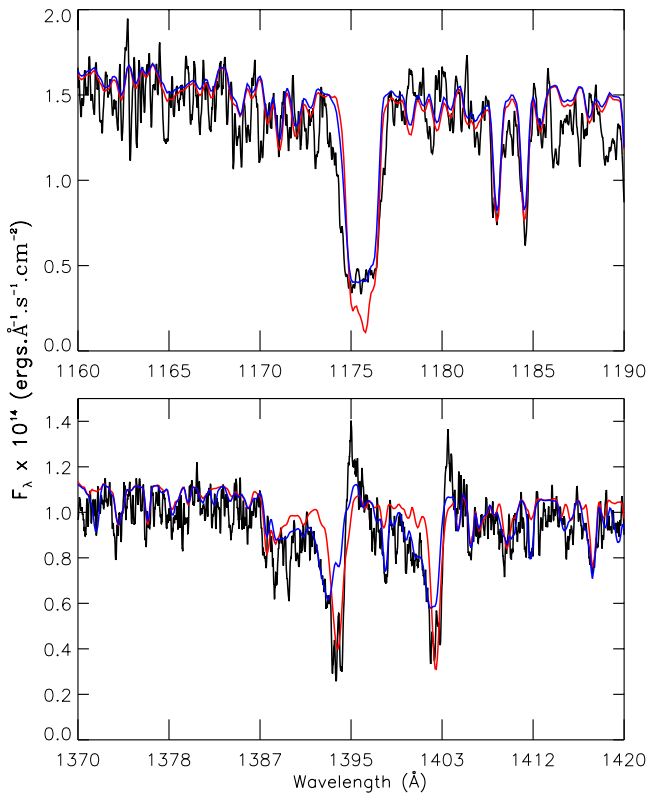


Figure 7. Profiles of C III $\lambda 1176$ (top) and Si IV resonance doublet (bottom). The model with \dot{M} varying with radius (see text and Fig. 6) is plotted in blue. Our best fit model is shown in red.

and a slight broadening, of the absorption associated with the Si IV resonance doublet. This blueshift and broadening is also seen in the C III triplet.

We thus argue that our mass-loss rate for A11 derived from the conventional lines is probably too low, by some factor between 3 and 10. Again, similar conclusions hold for B11. In these weak wind stars, the influence of porosity/vorosity effects, and the possible presence of hot gas, can potentially severely bias the estimated mass-loss rate.

9 WIND PROPERTIES AT LOW METALLICITY

From the modeling of the optical spectra of early-type stars, in three metal-deficient galaxies, more precisely galaxies with O/H less than SMC, Trammer et al. (2011, 2014) strikingly concluded that the mass-loss rates are consistent with those that would be predicted by the radiatively-driven wind theory for a higher, LMC-type, metal abundance. This led them to argue that this theory would break down at sub-SMC metallicity. If confirmed, this would be a major problem for our understanding of the physics of stellar winds, and for stellar evolution in the upper HRD as well. However, several facts suggest that the conclusion by Trammer et al. (2011, 2014) may be premature.

- We showed in Sect. 6 that the iron abundance in IC 1613 and WLM is higher than the metallicity adopted from O/H (Trammer et al. 2011, and refs therein). In the three stars, the metal content is not, if at all, significantly smaller than in the SMC, for which theoretical \dot{M} were found to match the empirical ones (Mokiem et al. 2007). The higher metal content shall impact the theoretical mass-loss rates as well as the wind terminal velocities, hence the modified wind-momentum-luminosity relation (WLR) for the stars⁵

- No important change in wind driving (e.g. going from a driving through lines of iron group elements to CNO) is expected until the metallicity is $1/50Z_{\odot}$ and below (Vink et al. 2001).

- Herrero et al. (2012) found that the wind parameters of an O6.5 IIIf star in IC 1613 are such that the star follows the WLR for its metallicity. In other words, if the metallicity would be sub-SMC (but see the recent conclusions by Garcia et al. 2014, besides ours), there is at least one case where the standard theory still applies.

- The sample analyzed by Trammer et al. (2014) contains 10 stars, a majority of them having wind strengths that are compatible with theory within the errors, assuming a SMC-like metal content. Only three stars (all of them in NGC 3109) are real outliers in the WLR diagram.

- The intrinsic dispersion in the wind parameters within a given spectral/luminosity class typically ranges within a factor of two. This is of the same amplitude as the difference that is expected for two stars with the same parameters but a factor of 2.5 in the metal content (i.e. going from LMC to SMC-type metallicity).

We showed in Sect. 5.1 and 5.2 that the FUV-spectra of IC 1613-A13, IC 1613-B11 and WLM-A11 indicate the presence of significant wind clumping. All other things being equal, the mass-loss rates quoted in Trammer et al. (2014) should therefore be reduced accordingly. The amplitude of the reduction depends on the nature of clumping (cf. Sect. 8.2); the typical reduction of \dot{M} found for clumped versus homogeneous models is found to be a factor 3 to 6. Clumped mass-loss rates are reduced by less than a factor of three compared to theoretical predictions (Bouret et al. 2012; Šurlan et al. 2013; Sundqvist et al. 2014). Note however that this last conclusion holds as long as the impact of clumping on the wind driving is not considered (see e.g. Muijres et al. 2011, for comments). Recently, Sundqvist et al. (2014) found that when applying a vorosity correction to the line force (based on the standard theory of line-driven winds by Castor et al. 1975), a reduction of the line force that drives the wind is obtained.

⁵ This relation links the modified wind momentum, defined as $D_{mom} = \dot{M} V_{\infty} \sqrt{R/R_{\odot}}$, to the stellar luminosity. The WLR is often used to study mass-loss in various galaxies and environments (e.g. Mokiem et al. 2007) as D_{mom} is almost independent of mass.

Therefore, a reduction of theoretical mass-loss rates is expected from these calculations if vorosity is present near the critical point, where the mass-loss rate is set. Such a scenario is supported by several observational (e.g. Puls et al. 2006; Najarro et al. 2011; Bouret et al. 2012) and theoretical (Cantiello et al. 2009; Sundqvist & Owocki 2013) results suggesting that clumping indeed starts close to the photosphere.

The mass-loss rates we derived using models with clumping are lower than those obtained from the modeling of the optical spectra only, especially for the late-type supergiants. We present in Fig. 8 the synthetic profiles of wind sensitive lines in the optical, namely the He II $\lambda 4686$ and H α line, as predicted with our values for \dot{M} and those obtained with CMFGEN for the parameters listed in (Tramper et al. 2014, their tables 4 and 5).

The H α line in IC1613-A13 are very similar in shape and strength, but a striking difference is observed in the predicted profiles for He II $\lambda 4686$. Even more striking is the fact this line is predicted in absorption by FASTWIND (Tramper et al. 2014, cf. figure 4 in), while the profile predicted by CMFGEN for the same parameters (and no clumping) shows clear electron scattering wings in emission. It is known however that CMFGEN often produces more emission in H α and He II $\lambda 4686$ than FASTWIND, for instance in the temperature and surface gravity regime corresponding to IC1613-A13 (e.g. Rivero González et al. 2012). In this regime, the formation of He II $\lambda 4686$ is very sensitive to radiative transfer effects, for instance the detailed treatment and amount of line-blanketing (model in green in Fig. 8 has much less elements than the best fit models), and the line profile responds accordingly.

Concerning the late-type supergiants IC1613-B11 and WLM-A11, the profiles predicted by CMFGEN for He II $\lambda 4686$ and H α for the two sets of parameters bracket the observed profiles. Since, admittedly, CMFGEN predicts stronger emission than FASTWIND in these lines, these profiles in Fig. 8 also likely bracket those which lead Tramper et al. (2011, 2014) to claim that mass-loss rates are higher than expected in IC1613 and WLM. We argue that, from such profiles only, it is quite uncertain what \dot{M} should be favored.

Despite the uncertainties on the real absolute values of mass-loss rates introduced by the feedback from clumping on line driving, the considerations spelled out hereabove suggest that the empirical mass-loss rates derived by Tramper et al. (2014) are likely overestimated, compared to those expected theoretical predictions and those derived by clumped models applied to the FUV + optical spectral range.

10 OBSERVED VERSUS PREDICTED MASS-LOSS RATES

10.1 Semi-empirical mass-loss rates

The mass-loss rates calculated for the stellar parameters using the recipe by Vink et al. (2001) are presented in Table 3. For the three stars, \dot{M} measured from FUV spectroscopy are lower than these estimates.

In the case of A13, the difference is slightly more than a factor of three, which is reasonable given the uncertainties on the photospheric and wind parameters derived from spectroscopy. Note that this difference would be slightly reduced if $Z = 0.14Z_{\odot}$ applies instead to the stars (by a factor $(0.2/0.14)^{0.69-0.83} = 1.28-1.34$), although the spectroscopic analysis does not support this lower value.

The mass-loss rate and clumping parameters of A13 are consistent with recent results obtained for SMC dwarfs (Bouret et al. 2013). The same behavior between measured and theoretical mass-loss rates is obtained for early type galactic dwarfs (Bouret et al. 2005; Martins et al. 2012) and supergiants (Bouret et al. 2012). All in all, this indicates that the wind properties of O stars of early spectral type are well accounted for by the standard theory of radiatively driven winds, regardless of the luminosity class and stellar metallicity. As for the wind terminal velocity, we note that our value $V_{\infty} = 2180 \text{ km s}^{-1}$ is much higher than $V_{\infty} \approx 1570 \text{ km s}^{-1}$, inferred from the usual scaling $V_{\infty}/v_{esc} = 2.6$ (Kudritzki & Puls 2000), then to the star's metallicity $V_{\infty} \propto Z^{0.13}$ (Leitherer et al. 1992). It is important to recall that in the recipe by Vink et al. (2001), the wind velocity structure and terminal velocity are adopted as input to predict the mass-loss rate. Said differently, the adopted value for V_{∞} impacts the mass-loss prediction. A difference in V_{∞} such as the one we find for A13 implies a difference of more than 0.28 dex in the theoretical mass-loss rates, all other parameter being equal.

The case for B11 and A11 is different. The terminal velocities we measure are in good agreement (within 50 km s^{-1}) with the values predicted using the theoretical scaling between surface escape velocity and wind terminal velocity, then with metallicity (for the derived stellar parameters and iron abundance). On the other hand, the mass-loss rates are much lower than predicted by the recipe from Vink et al. (2001) for these stellar parameters and the iron abundance. The discrepancy reaches up to a factor of twenty and thirty five for B11 and A11 (resp.), assuming a SMC-type metallicity for IC 1613 and WLM. In order to reconcile the measured mass-loss rates with theoretical values, the metallicities would need to be $Z = 0.03Z_{\odot}$ and $0.002Z_{\odot}$ for B11 and A11 respectively. Such low metallicities are clearly ruled out by the spectroscopic analysis (as is $Z = 0.14Z_{\odot}$, which would only marginally reduce the discrepancy between observed and theoretical \dot{M} anyway). Of course, this discrepancy is very likely an upper limit, should the true mass-loss rates be revised upward for A11 and B11 as a result of a proper treatment of porosity/vorosity effects (cf. Sect. 8). Note also that in the specific case of A11, the difference could be reduced though, adopting a luminosity and a mass more in line with those expected for a normal O9.7 supergiant, to compute the theoretical mass-loss rate (e.g. $\log \frac{L}{L_{\odot}} = 5.5$ and $M=31M_{\odot}$, from Martins et al. 2005). When corrected for this luminosity effect, possibly indicating a binary/multiple status for this star, the difference with the theoretical \dot{M}_{Vink} is of the same amplitude as for B11.

In any case, even though our modeling concurs with Tramper et al. (2011, 2014) that the measured mass-loss rates of B11 and A11 disagree with theoretical predictions, *we find the discrepancy to occur in the opposite sense.*

Recently, Muijres et al. (2012) built on the work by Müller & Vink (2008) to compute new mass-loss rates and terminal wind velocities, improving the physics implemented in the Monte-Carlo (MC) method used by Vink et al. (2000, 2001). In this new approach, a parametrized description for the line acceleration is used to derive new expression for the velocity field of a radiation-driven wind. A major conclusion of this work is that for stars more luminous than $\log \frac{L}{L_{\odot}} \geq 5.2$, the new mass-loss rates and those by Vink et al. (2000) agree well. On the other hand, for physical parameters relevant to a typical late-type O supergiant (i.e. close to those of B11 and A11), the new mass-loss rates are between 0.3 – 0.4 dex lower than those computed by Vink et al. (2000). The wind terminal velocities however, are notably higher than observed for such objects (e.g. Howarth & Prinja 1989). Notwithstanding

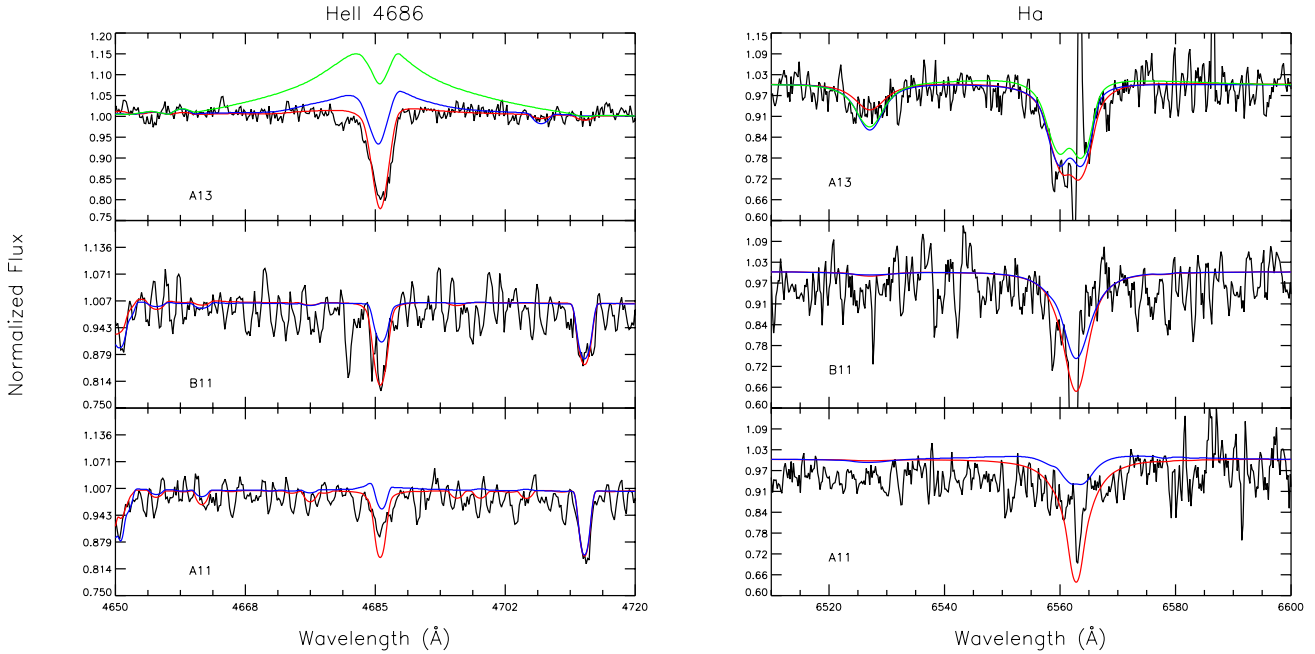


Figure 8. Left: In black, the spectral region around the He II $\lambda 4686$ line, observed for IC1613-A13, B11 and WLM-A11 (from top to bottom). Synthetic profiles produced by models computed with CMFGEN using the parameters from Tramper et al. (2014) and those derived from the joint FUV+optical analysis presented here are overplotted (in blue and red, respectively). Right: Same, from the region around the H α line. The model in green presented for IC1613-A13 illustrates the sensitivity of the He II $\lambda 4686$ line to line-blanketing (Ne, Cl, Ar, Ca are not included) while the H α line is much less affected.

the possible reasons for these over-predicted V_∞ (see Muijres et al. 2012, for a discussion), these MC simulations essentially predict the total wind kinetic energy $\dot{M}V_\infty^2$, and any change in the wind terminal speed reflects in a change in the mass-loss rate, hence the observed decrease of \dot{M} . More quantitative comparison to B11 and A11 is not possible, however, because the mass-loss rates and wind terminal velocities have been computed by Muijres et al. (2012) for galactic metallicity only. Assuming that the theoretical scaling obtained by Vink et al. (2001) still holds, the mass-loss rate should be scaled down by another 0.5 dex, while V_∞ would change by less than 20%, compared to the galactic values. With a total scale down of $\approx 0.8 - 0.9$ dex, \dot{M} would still be a factor of three to five higher than measured from FUV spectroscopy. Furthermore, if the V_∞ for these late-type supergiants are much lower (as we measure them) than predicted (40% typically), then the theoretical \dot{M} should go up. It is not clear that mass-loss prediction at different metallicities, based on Muijres et al. (2012) improvement in the treatment of the line force parametrization, would be able to account for the observed mass-loss rates of B11 and A11.

10.2 Mass fluxes obtained by solving the dynamics of radiatively-driven winds

Lucy (2010b) argued that the mass-loss rates by Vink et al. (2001) that have been compared to observations, may not be relevant for such comparisons because they are derived by imposing a global dynamical constraint, i.e. assuming that the energy that is needed to drive the wind is indeed extracted from the radiation field, rather than being obtained by solving the equations governing the dynamics of radiatively-driven winds. In order to fully guarantee that the derived mass-loss rates are consistent with stationary transonic flows, Lucy (2010b) computed mass fluxes that allow the wind mass flow to accelerate continuously from sub- to supersonic ve-

locities. The theory of moving reversing layers (MRL) pioneered by Lucy & Solomon (1970) was used to determine the mass fluxes from first principles by imposing a regularity condition at the sonic point. An important conclusion from this work was that the so-called *weak-wind problem* mostly arises from the existence of two separate regimes of ionization of iron. More precisely, a shift in the ionization balance of iron, from Fe V to Fe IV (as T_{eff} decreases), leads to weaker line acceleration below the sonic point, which translates into lower mass-loss rates. In the temperature domain of late O-type stars, namely $T_{\text{eff}} \approx 30,000$ K, the Fe V contribution to the driving is dramatically reduced and a reduction by up to ≈ 1.4 dex is obtained compared to mass-loss rates predicted by Vink et al. (2000)⁶.

More recently, Lucy (2012) extended this work to predict mass fluxes that depend on the stellar metallicity, without relying on scaling laws (e.g. Vink et al. 2001; Mokiev et al. 2007) but implementing curve-of-growth effects in the dynamic of the reversing layers instead. Mass fluxes computed with this method present manifest departure from the expected, linear, monotonic, decline with metallicity (see Fig. 1 in Lucy 2012). It is noteworthy that the strongest departure from a (single) power-law scaling is found for the metallicity and $(T_{\text{eff}} - \log g)$ regime of the two late-type supergiants IC 1613-B11 and WLM-A11.

We used the value listed in Table 1 from Lucy (2012) to calculate the mass-loss rates corresponding to the stellar parameters we derive for IC1613-A13, IC1613-B11 and WLM-A11 respectively. It is fortunate that the case for $T_{\text{eff}} = 42,500$ K and $\log g = 3.75$ was also worked out by Lucy (2012) as it best account for the parameters of IC1613-A13 as derived in the present study. The results are

⁶ Muijres et al. (2012) do solve the full momentum equation, but they now obtain that for stars having $\log \frac{L}{L_\odot} \geq 5.2$, i.e. stars in the “*weak wind*” regime, their hydrodynamical method fails to drive a wind.

summarized in Table 3. The striking conclusion from this comparison is that, while the good match between theoretical and observed \dot{M} for IC 1613-A13 is maintained, the discrepancy between observed and theoretical mass-loss rates we found for IC1613-B11 and WLM-A11 when using mass-loss rates from Vink et al. (2001) is dramatically reduced (and would be even more if mass-loss rates are higher by a factor of 3 to 10, as discussed in Sect .8). Quantitatively, the theoretical \dot{M}_{Lucy} of B11 and A11 are more than one order of magnitude less than \dot{M}_{Vink} . For a large part, this is a consequence of the aforementioned reduction of line-driving caused by the lower ionization of iron. The amplitude of the decrease is an additional balance between the decreased contribution of Fe (and Ni for that matter) to the driving and an enhancement of \dot{M} caused by the lower surface gravities (see Sect. 4 and 5 in Lucy 2010a, for a discussion). The remaining differences are well within the uncertainties caused by the cumulative effects of error on the measured stellar and wind parameters (especially the impact of clumping on the driving) on one hand, and in input abundances (global scaling to solar values) and micro turbulence velocity from the TLUSTY models of Lanz & Hubeny (2003) used by Lucy (2012) to compute mass fluxes.

Interestingly, Lucy (2012) found no dynamically consistent solutions that would yield higher mass fluxes, within the purely radiation-driven winds framework, to provide better agreement with the mass-loss rates by Trammer et al. (2011). An (yet unknown) additional driving mechanism would be therefore required to provide more radiative acceleration. With \dot{M} derived from FUV spectroscopy, such a putative mechanism may not be needed anymore.

10.3 Modified Wind-Momentum-Luminosity Relation

Using the FUV-measured mass-loss, and those computed with Vink et al. (2001) and Lucy (2012), we built the modified wind-momentum-luminosity (see e.g. Kudritzki & Puls 2000) relation for the three stars (Fig. 9). We further added the modified wind-momenta (D_{mom} cf. Sect. 9) obtained for mass-loss rates predicted by both approaches for A11 assuming a lower luminosity (hence radius) for this object. Recall that this assumption is based on considerations on measured surface gravity, which yield abnormally high spectroscopic mass for this object, if the luminosity deduced from the SED fitting of observed fluxes is used. Measured wind-momenta are clearly lower (more than one order of magnitude for B11 and A11) than predicted using the theoretical coefficients (Vink et al. 2001) for the WLR of the LMC and SMC metallicities (see caption for details). For the stellar coefficients derived from spectroscopy, the mass-loss rates predicted by Vink et al. (2001) yield D_{mom} that are (expectedly) in better agreement with the theoretical relations, although some striking differences are observed. Note the case of IC1613-A13, where the predicted D_{mom} is more compatible with the theoretical WLR for LMC. The predicted D_{mom} for WLM-A11 is below the theoretical relation but the agreement would be much improved assuming that WLM-A11 has a $\log L/L_{\odot}$ lower by 0.2 dex.

Although the small number of points makes further quantitative interpretation questionable, we argue that wind properties derived from FUV diagnostics are better accounted for by the MRL approach. The above comparisons strongly suggest that the information on wind quantities available in the optical spectra in Trammer et al. (2011, 2014) is probably too limited and the FUV provides more realistic estimates, while a proper treatment of the radiatively-driven winds dynamics considerably improves the calculation of

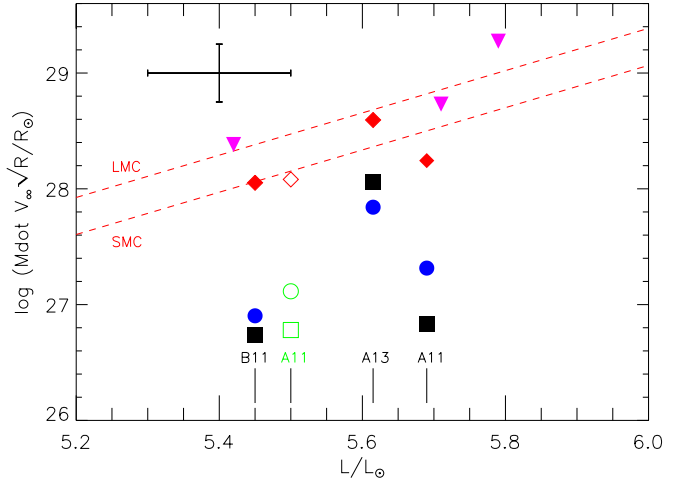


Figure 9. Modified wind-momentum luminosity relation for the sample stars. Black full squares mark D_{mom} calculated for the spectroscopic parameters listed in Table 3. Blue full circles are D_{mom} calculated with the mass fluxes from Lucy (2012) for the stellar parameters, while red full diamonds are D_{mom} computed with the Vink et al. (2001) recipe. D_{mom} for WLM-A11 assuming $\log L/L_{\odot} = 5.5$ are indicated as empty symbols (same shape and color coding as previously). The dashed red lines are the theoretical relation for LMC and SMC metallicities predicted by Vink et al. (2000). Pink triangles are D_{mom} from Trammer et al. (2014) for the three stars. For clarity, no individual error bars are given but we plot a typical error bar on the upper left corner.

mass fluxes. The remaining discrepancies between the observed and theoretical mass-loss rates for A13, B11 and A11 reflects the many uncertainties related to simplifications that are made both in the diagnostic models and in theoretical calculation of mass-loss rates. The mass-loss – metallicity scaling breakdown at sub-SMC metallicity is not confirmed at this step.

11 SUMMARY AND CONCLUSIONS

We have modeled the FUV spectra of three O stars in the low metallicity galaxies IC 1613 and WLM, observed with HST/COS. Our goal was to corroborate or refute the results by Trammer et al. (2011, 2014) suggesting that the mass-loss rates of some of these stars are more compatible with higher metallicity and similar to those of LMC stars. This result, if upheld, would have far-reaching consequences beyond our understanding of radiatively-driven winds, and would impact for instance the predicted number of collapsars and of SN Ib and Ic in low metallicity environments, hence in the high- z Universe.

Because of numerous iron lines and lines sensitive to wind properties, FUV spectroscopy is the adequate tool to fully address and resolve this outstanding issue of the dependence of hot, massive star mass-loss rates with metallicity. A comparison of these new COS spectra with exsistant STIS or COS spectra of Galactic, LMC and SMC stars provided a direct, model-independent check of the mass-loss - metallicity relation. A quantitative analysis was then carried out using state-of-the-art NLTE unified model atmospheres calculated with the CMFGEN code to establish the wind properties of the three low-metallicity massive stars.

- The spectroscopic analysis indicates that the metallicity of the three targets is $1/5Z_{\odot}$, i.e. SMC-like, although the usual value

adopted for IC1613 and WLM of $Z = 1/7Z_{\odot}$ is not ruled out. Lower and higher values of the metal content ($1/10Z_{\odot}$ and $1/2Z_{\odot}$ respectively) are not consistent with the observed spectra.

- The FUV data allow secure inferences on the CNO abundances, of critical importance for mass-loss rates determinations.

- The wind parameters derived from the FUV-spectroscopic analysis of the observed HST/COS spectra provide very satisfactory fits to the optical spectra as well. This further illustrates the limitations related to \dot{M} determinations based on the optical spectrum ($H\alpha$) only.

- The mass-loss rates differ from those derived by Tramper et al. (2011, 2014). The difference for IC1613-A13 is moderate (less than a factor of 6), and it can be accounted for by clumping (and to some extent to the detailed treatment and amount of line-blanketing). For the late-type supergiants (IC1613-B11 and WLM-A11), the amplitude of the difference is much higher, reaching from ~ 1.6 to 2.5 orders of magnitude, respectively. Here, wind clumping (absent in the analysis of the optical spectra) might account for a factor of three in the difference only. A combination of several other factors can explain the rest of the difference : (i) In these weak wind stars, the influence of porosity/vorosity effects, and the possible presence of hot gas, can potentially bias the estimated mass-loss rate by factors from 3 to 10; (ii) In the region of parameter space corresponding to these stars, CMFGEN and FASTWIND produce systematically different results for optical lines, with more emission/infill predicted by CMFGEN.

- For the re-visited metallicity, we find that the mass-loss rates of IC1613-A13, the earliest star of the sample, is in good agreement with the mass-loss predicted with the recipe by Vink et al. (2001). The C IV P Cygni profile of A13, which is stronger than that of the SMC dwarf MPG 324 (cf. Fig. 2) is probably a consequence of its more evolved status.

- On the other hand, \dot{M} measured with FUV spectra for IC1613-B11 and WLM-A11, two late-type O supergiants, are clearly lower than measured in the optical by Tramper et al. (2014). Because of the systematic errors, they may however be consistent with the theoretical predictions by Vink et al. (2001) for the preferred metallicities. If the later is true, porosity/vorosity effects and the state of the gas (i.e., what fraction is hot) are of crucial importance.

- We used a different approach to calculate mass-loss rates, as outlined recently in Lucy (2012). With this alternative method, avoiding scaling laws and assumptions on the terminal wind velocities, the measured mass-loss rates of the three stars are then in much better agreement with theoretical values. We therefore conclude that there is no indication at this moment that the radiatively-driven wind theory breaks down at metallicities at or slightly less than SMC values.

Our results are restricted to a very limited number of objects. We pointed out that the observed mass-loss rates within a spectral/luminosity class may vary within a factor of four or more just because of the scatter of the intrinsic individual parameters. To reach a firm conclusion on the nature of the $\dot{M}(Z)$ relation therefore requires larger statistical sample, preferentially observed in the FUV at (relatively) high spectral resolution and high signal-to-noise ratio, to simultaneously derive the iron content and the wind parameters. This, unfortunately, is beyond routine capability of HST for galaxies more distant than the MCs. On the other hand, a fairly decent sample of objects is available in the HST archives for stars in the SMC and we shall now focus on these objects to study the properties of stellar winds at low metallicity. We engaged in such a study and results will be presented in a coming paper

discussing the properties of mass-loss for stars from dwarfs to supergiants.

ACKNOWLEDGEMENTS

We thank an anonymous referee for a careful reading and suggestions which help improve this paper. We thank Joachim Puls for computing a FASTWIND model for us and for discussion about wind sensitive optical lines. J.-C. Bouret is indebted to S. R. Heap for her invitation to work at NASA/GSFC when this work was initiated (work was supported by NASA grant NNX08AC146 to the University of Colorado at Boulder). DJH acknowledges support from STScI GO grant HST-GO- 12867.001-A and STScI theory grant HST-AR- 12640.01. We acknowledge financial support from “Programme National de Physique Stellaire” (PNPS) of CNRS/INSU, France. This research has made use of the SIMBAD database, operated at CDS, Strasbourg, France.

REFERENCES

- Asplund M., Grevesse N., Sauval A. J., 2005, in Barnes III T. G., Bash F. N., eds, *Cosmic Abundances as Records of Stellar Evolution and Nucleosynthesis Vol. 336 of Astronomical Society of the Pacific Conference Series, The Solar Chemical Composition*. pp 25–4
- Bouret J.-C., Hillier D. J., Lanz T., Fullerton A. W., 2012, *A&A*, 544, A67
- Bouret J.-C., Lanz T., Hillier D. J., 2005, *A&A*, 438, 301
- Bouret J.-C., Lanz T., Hillier D. J., Heap S. R., Hubeny I., Lennon D. J., Smith L. J., Evans C. J., 2003, *ApJ*, 595, 1182
- Bouret J.-C., Lanz T., Martins F., Marcolino W. L. F., Hillier D. J., Depagne E., Hubeny I., 2013, *A&A*, 555, A1
- Bresolin F., Pietrzyński G., Urbaneja M. A., Gieren W., Kudritzki R.-P., Venn K. A., 2006, *ApJ*, 648, 1007
- Bresolin F., Urbaneja M. A., Gieren W., Pietrzyński G., Kudritzki R.-P., 2007, *ApJ*, 671, 2028
- Busche J. R., Hillier D. J., 2005, *AJ*, 129, 454
- Cantiello M., Langer N., Brott I., de Koter A., Shore S. N., Vink J. S., Voegler A., Lennon D. J., Yoon S.-C., 2009, *A&A*, 499, 279
- Cardelli J. A., Clayton G. C., Mathis J. S., 1989, *ApJ*, 345, 245
- Castor J. I., Abbott D. C., Klein R. I., 1975, *ApJ*, 195, 157
- Cole A. A., Tolstoy E., Gallagher J. S., et al., 1999, *AJ*, 118, 1657
- Crowther P. A., Schnurr O., Hirschi R., Yusof N., Parker R. J., Goodwin S. P., Kassim H. A., 2010, *MNRAS*, 408, 731
- David-Uraz A., Wade G. A., Petit V., ud-Doula A., Sundqvist J. O., Grunhut J., Shultz M., Neiner C., Alecian E., Henrichs H. F., Bouret J.-C., MiMeS Collaboration 2014, *MNRAS*, 444, 429
- de Koter A., Heap S. R., Hubeny I., 1998, *ApJ*, 509, 879
- Drew J. E., Hoare M. G., Denby M., 1994, *MNRAS*, 266, 917
- Evans C. J., Lennon D. J., Smartt S. J., Trundle C., 2006, *A&A*, 456, 623
- Freyer T., Hensler G., Yorke H. W., 2003, *ApJ*, 594, 888
- Garcia M., Herrero A., Najarro F., Lennon D. J., Alejandro Urbaneja M., 2014, *ApJ*, 788, 64
- Garcia M., Herrero A., Vicente B., Castro N., Corral L. J., Rosenberg A., Monelli M., 2009, *A&A*, 502, 1015
- Garcia M., Najarro F., Herrero A., Urbaneja M. A., Lennon D. J., Castro N., 2013, in *Massive Stars: From alpha to Omega*

- Winds of Very Low Metallicity OB Stars: Beyond the Magellanic Clouds. p. 66
- Hamann W.-R., 1981, *A&A*, 93, 353
- Heap S. R., Lanz T., Hubeny I., 2006, *ApJ*, 638, 409
- Herrero A., Garcia M., Puls J., Uytterhoeven K., Najarro F., Lennon D. J., Rivero-González J. G., 2012, *A&A*, 543, A85
- Hillier D. J., Kudritzki R. P., Pauldrach A. W., Baade D., Cassinelli J. P., Puls J., Schmitt J. H. M. M., 1993, *A&A*, 276, 117
- Hillier D. J., Lanz T., Heap S. R., Hubeny I., Smith L. J., Evans C. J., Lennon D. J., Bouret J. C., 2003, *ApJ*, 588, 1039
- Hillier D. J., Miller D. L., 1998, *ApJ*, 496, 407
- Hillier D. J., Miller D. L., 1999, *ApJ*, 519, 354
- Holland S. T., Oskinova L. M., Ignace R., Waldron W. L., Todt H., Hamaguchi K., Kitamoto S., 2012, *Cosmic Origins Spectrograph Instrument Handbook for Cycle 21 v. 5.0*
- Howarth I. D., Prinja R. K., 1989, *ApJS*, 69, 527
- Huenemoerder D. P., Oskinova L. M., Ignace R., Waldron W. L., Todt H., Hamaguchi K., Kitamoto S., 2012, *ApJL*, 756, L34
- Kudritzki R. P., Puls J., 2000, *ARA&A*, 38, 613
- Lamers H. J. G. L. M., Cerruti-Sola M., Perinotto M., 1987, *ApJ*, 314, 726
- Lanz T., Hubeny I., 2003, *ApJS*, 146, 417
- Leitherer C., Robert C., Drissen L., 1992, *ApJ*, 401, 596
- Lucy L. B., 2010a, *A&A*, 524, A41
- Lucy L. B., 2010b, *A&A*, 512, A33
- Lucy L. B., 2012, *A&A*, 543, A18
- Lucy L. B., Solomon P. M., 1970, *ApJ*, 159, 879
- Maeder A., Meynet G., 2001, *A&A*, 373, 555
- Marcolino W. L. F., Bouret J.-C., Martins F., Hillier D. J., Lanz T., Escolano C., 2009, *A&A*, 498, 837
- Martins F., Depagne E., Russeil D., Mahy L., 2013, *A&A*, 554, A23
- Martins F., Hillier D. J., 2012, *A&A*, 545, A95
- Martins F., Mahy L., Hillier D. J., Rauw G., 2012, *A&A*, 538, A39
- Martins F., Plez B., 2006, *A&A*, 457, 637
- Martins F., Schaerer D., Hillier D. J., 2005, *A&A*, 436, 1049
- Martins F., Schaerer D., Hillier D. J., Meynadier F., Heydari-Malayeri M., Walborn N. R., 2005, *A&A*, 441, 735
- Mason B. D., Hartkopf W. I., Gies D. R., Henry T. J., Helsel J. W., 2009, *AJ*, 137, 3358
- Massa D., Oskinova L. M., Ignace R., Waldron W. L., Todt H., Hamaguchi K., Kitamoto S., 2013, *COS Data Handbook v. 2.0*
- Massey P., Bresolin F., Kudritzki R. P., Puls J., Pauldrach A. W. A., 2004, *ApJ*, 608, 1001
- Massey P., Olsen K. A. G., Hodge P. W., Jacoby G. H., McNeill R. T., Smith R. C., Strong S. B., 2007, *AJ*, 133, 2393
- Massey P., Puls J., Pauldrach A. W. A., Bresolin F., Kudritzki R. P., Simon T., 2005, *ApJ*, 627, 477
- Massey P., Zangari A. M., Morrell N. I., Puls J., DeGioia-Eastwood K., Bresolin F., Kudritzki R., 2009, *ApJ*, 692, 618
- McConnachie A. W., Irwin M. J., Ferguson A. M. N., Ibata R. A., Lewis G. F., Tanvir N., 2005, *MNRAS*, 356, 979
- Meynet G., Maeder A., 2005, *A&A*, 429, 581
- Minniti D., Zijlstra A. A., 1997, *AJ*, 114, 147
- Mokiem M. R., de Koter A., Evans C. J., Puls J., Smartt S. J., Crowther P. A., Herrero A., Langer N., Lennon D. J., Najarro F., Villamariz M. R., Yoon S., 2006, *A&A*, 456, 1131
- Mokiem M. R., de Koter A., Vink J. S., Puls J., Evans C. J., Smartt S. J., Crowther P. A., Herrero A., Langer N., Lennon D. J., Najarro F., Villamariz M. R., 2007, *A&A*, 473, 603
- Muijres L. E., de Koter A., Vink J. S., Krtićka J., Kubát J., Langer N., 2011, *A&A*, 526, A32
- Muijres L. E., Vink J. S., de Koter A., Müller P. E., Langer N., 2012, *A&A*, 537, A37
- Müller P. E., Vink J. S., 2008, *A&A*, 492, 493
- Najarro F., Hanson M. M., Puls J., 2011, *A&A*, 535, A32
- Oskinova L. M., Hamann W.-R., Feldmeier A., 2007, *A&A*, 476, 1331
- Owocki S. P., Castor J. I., Rybicki G. B., 1988, *ApJ*, 335, 914
- Owocki S. P., Sundqvist J. O., Cohen D. H., Gayley K. G., 2013, *MNRAS*, 429, 3379
- Pietrzyński G., Gieren W., Soszyński I., Bresolin F., Kudritzki R.-P., Dall'Ora M., Storm J., Bono G., 2006, *ApJ*, 642, 216
- Prinja R. K., 1998, in Kaper L., Fullerton A. W., eds, *Cyclical Variability in Stellar Winds Systematic Variability in Ob-Star Winds*. pp 92+
- Prinja R. K., Crowther P. A., 1998, *MNRAS*, 300, 828
- Puls J., Kudritzki R.-P., Herrero A., Pauldrach A. W. A., Haser S. M., Lennon D. J., Gabler R., Voels S. A., Vilchez J. M., Wachter S., Feldmeier A., 1996, *A&A*, 305, 171
- Puls J., Markova N., Scuderi S., Stanghellini C., Taranova O. G., Burnley A. W., Howarth I. D., 2006, *A&A*, 454, 625
- Puls J., Urbaneja M. A., Venero R., Repolust T., Springmann U., Jokuthy A., Mokiem M. R., 2005, *A&A*, 435, 669
- Puls J., Vink J. S., Najarro F., 2008, *A&ARv*, 16, 209
- Rivero González J. G., Puls J., Massey P., Najarro F., 2012, *A&A*, 543, A95
- Rivero González J. G., Puls J., Najarro F., 2011, *A&A*, 536, A58
- Runacres M. C., Owocki S. P., 2002, *A&A*, 381, 1015
- Sana H., de Koter A., de Mink S. E., Dunstall P. R., Evans C. J., Henault-Brunet V., Maiz Apellaniz J., Ramirez-Agudelo O. H., Taylor W. D., Walborn N. R., Clark J. S., Crowther P. A., Herrero A., Gieles M., Langer N., Lennon D. J., Vink J. S., 2012, *ArXiv e-prints*
- Sana H., Le Bouquin J.-B., Lacour S., Berger J.-P., Duvert G., Gauchet L., Norris B., Olofsson J., Pickel D., Zins G., Absil O., de Koter A., Kratter K., Schnurr O., Zinnecker H., 2014, *ApJS*, 215, 15
- Sana H., Rauw G., Nazé Y., Gosset E., Vreux J., 2006, *MNRAS*, 372, 661
- Simón-Díaz S., 2010, *A&A*, 510, A22+
- Skillman E. D., Tolstoy E., Cole A. A., Dolphin A. E., Saha A., Gallagher J. S., Dohm-Palmer R. C., Mateo M., 2003, *ApJ*, 596, 253
- Sundqvist J. O., Owocki S. P., 2013, *MNRAS*, 428, 1837
- Sundqvist J. O., Puls J., Feldmeier A., Owocki S. P., 2011, *A&A*, 528, A64+
- Sundqvist J. O., Puls J., Owocki S. P., 2014, *A&A*, 568, A59
- Tautvaišienė G., Geisler D., Wallerstein G., Borissova J., Bizyaev D., Pagel B. E. J., Charbonnel C., Smith V., 2007, *AJ*, 134, 2318
- Tramper F., Sana H., de Koter A., Kaper L., 2011, *ApJL*, 741, L8
- Tramper F., Sana H., de Koter A., Kaper L., Ramírez-Agudelo O. H., 2014, *A&A*, 572, A36
- Urbaneja M. A., Kudritzki R.-P., Bresolin F., Przybilla N., Gieren W., Pietrzyński G., 2008, *ApJ*, 684, 118
- Šurlan B., Hamann W.-R., Aret A., Kubát J., Oskinova L. M., Torres A. F., 2013, *A&A*, 559, A130
- Venn K. A., Tolstoy E., Kaufer A., Skillman E. D., Clarkson S. M., Smartt S. J., Lennon D. J., Kudritzki R. P., 2003, *AJ*, 126, 1326
- Villamariz M. R., Herrero A., 2000, *A&A*, 357, 597
- Vink J. S., de Koter A., Lamers H. J. G. L. M., 2000, *A&A*, 362, 295

- Vink J. S., de Koter A., Lamers H. J. G. L. M., 2001, *A&A*, 369, 574
Woosley S. E., 1993, *ApJ*, 405, 273
Yoon S., Langer N., 2005, *A&A*, 443, 643
Zsargó J., Hillier D. J., Bouret J., Lanz T., Leutenegger M. A., Cohen D. H., 2008, *ApJL*, 685, L149

APPENDIX A: BEST FITS

In this appendix we compare our best-fit models to the optical and UV spectra. Absolute fluxes in UV spectra are provided after correcting for reddening (see Sect. 4) and are expressed in $\text{ergs} \cdot \text{\AA}^{-1} \cdot \text{s}^{-1} \cdot \text{cm}^{-2}$.

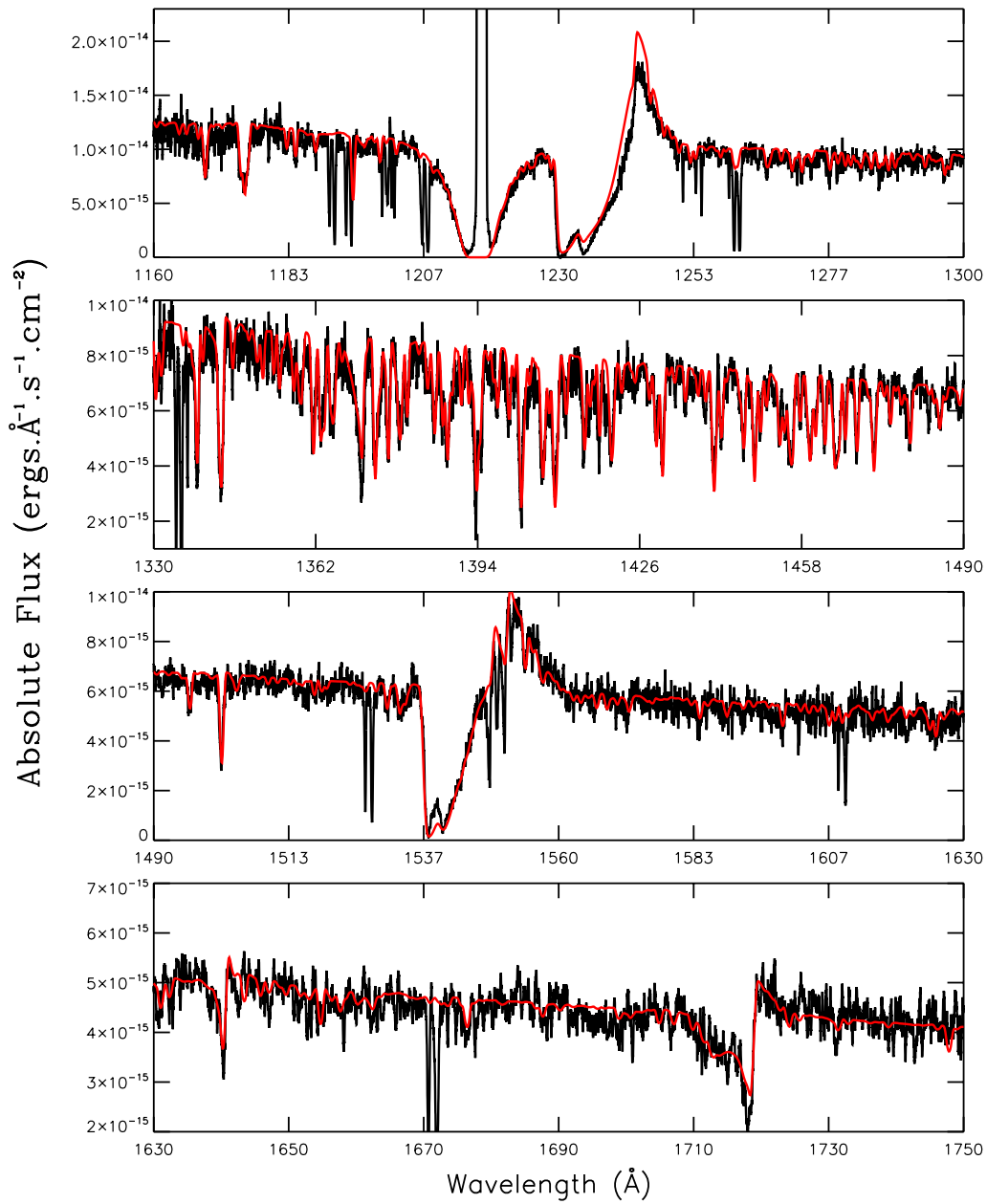


Figure A1. FUV spectrum of IC 1613-A13 (in black). Overplotted in red is the best fit model (see text for comments). A satisfactory fit is obtained for the observed photospheric (mainly Fe forest) and wind profiles. In particular, the N v $\lambda 1240$ and N iv $\lambda 1718$ wind profiles are well reproduced, indicating correct ionization fractions in the wind.

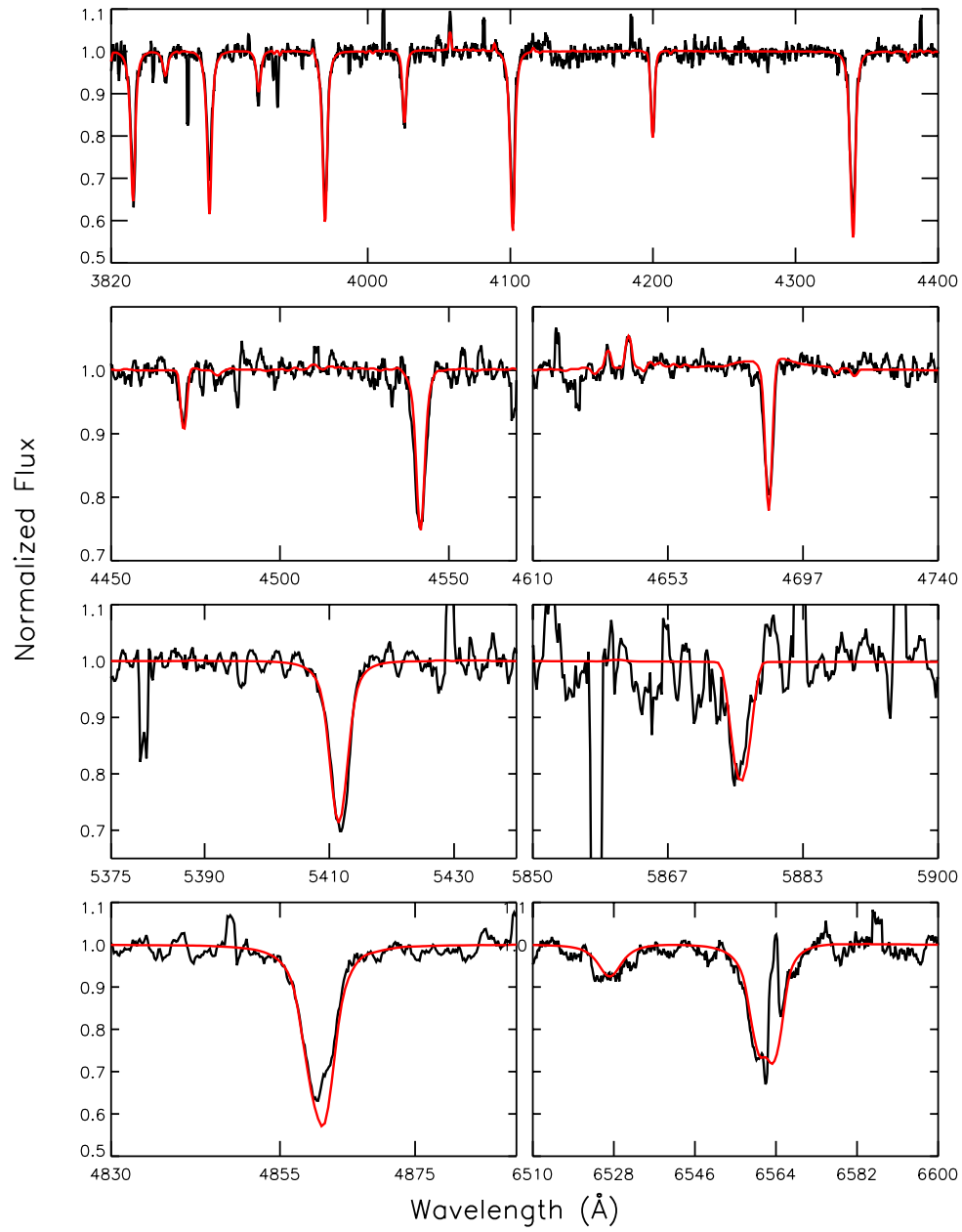


Figure A2. Optical spectrum of IC 1613-A13. Overplotted in red is the best fit model (see text for comments).

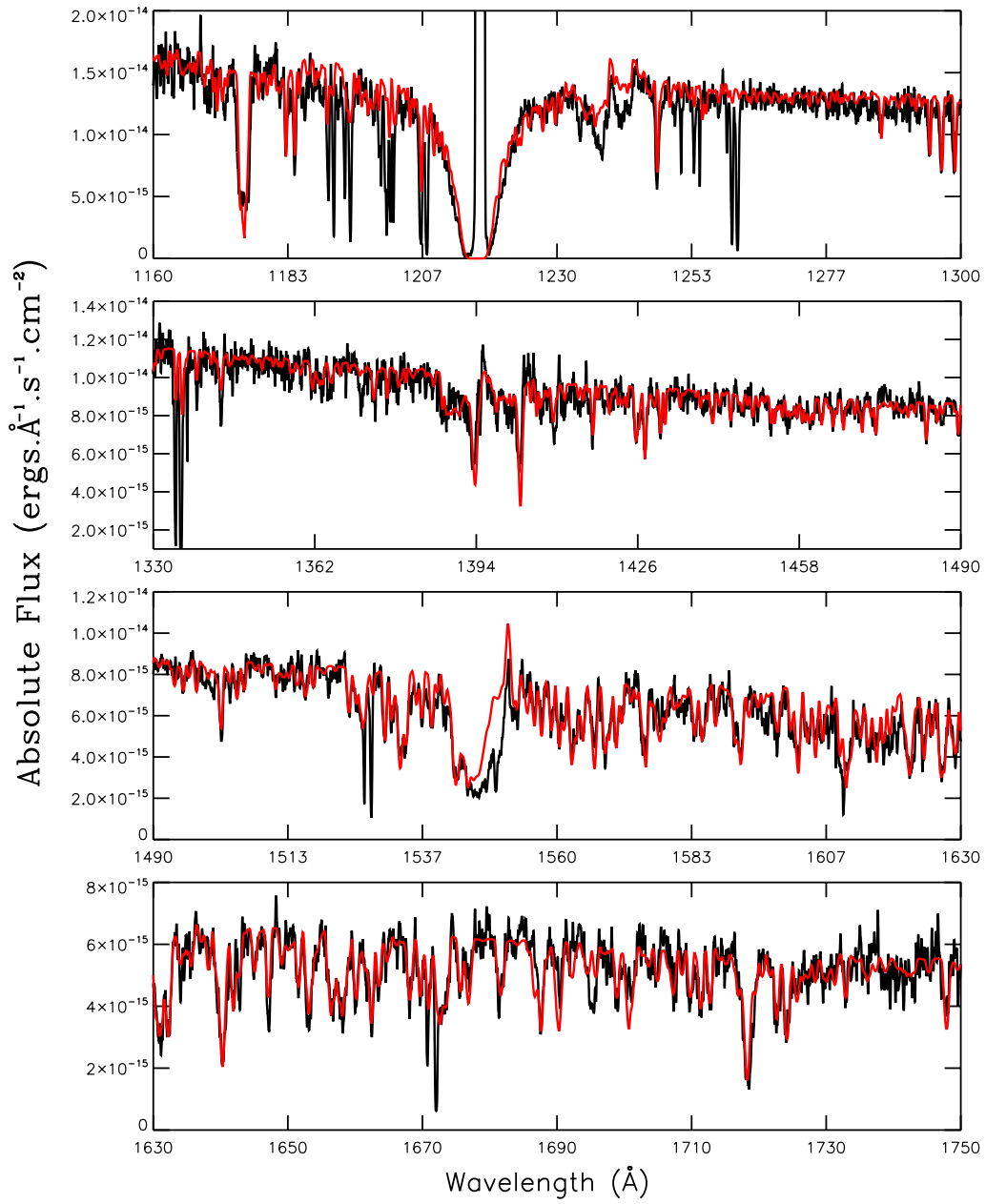


Figure A3. FUV spectrum of IC 1613-B11 (in black). Overplotted in red is the best fit model (see text for comments).

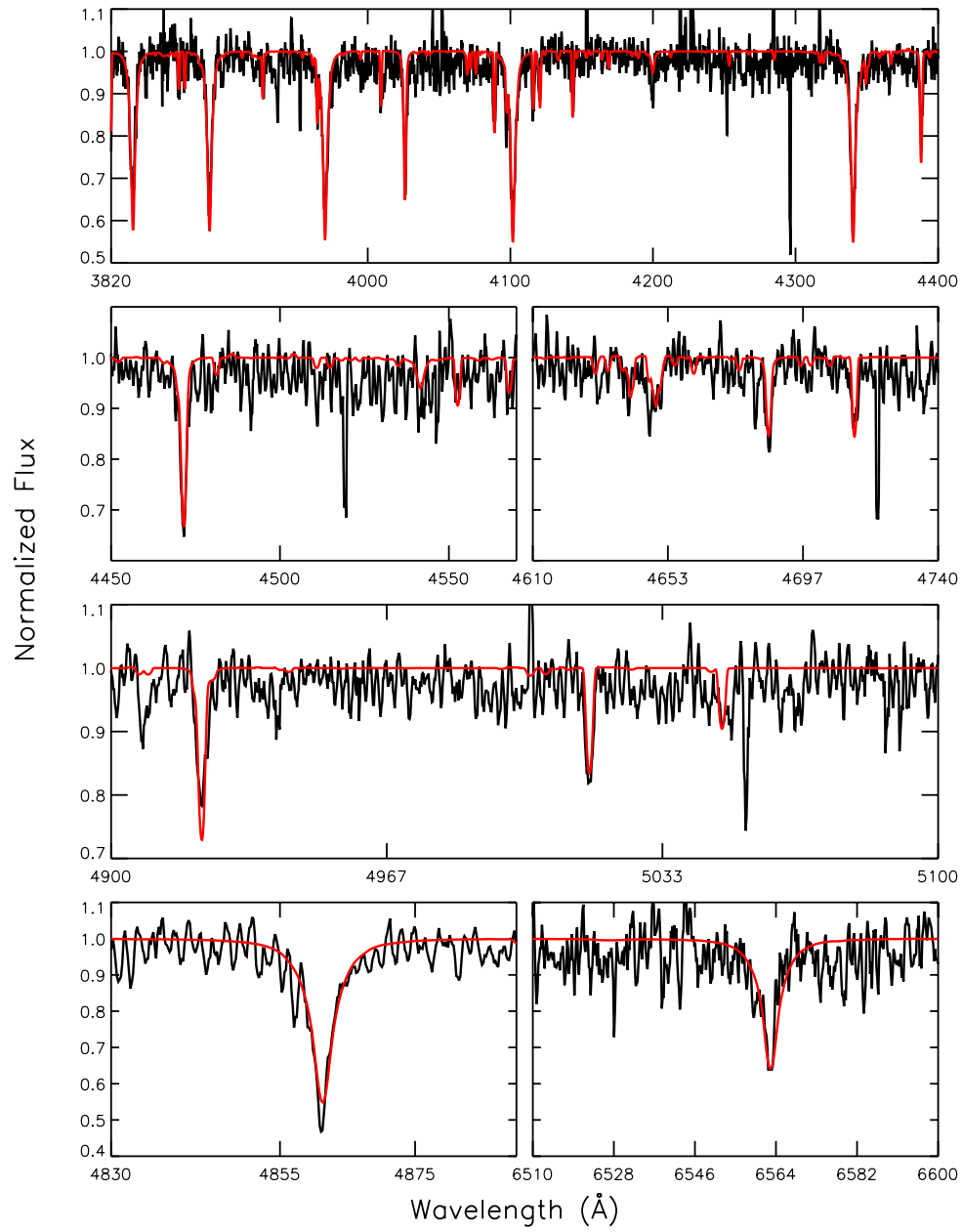


Figure A4. Optical spectrum of IC 1613-B11. Overplotted in red is the best fit model (see text for comments).

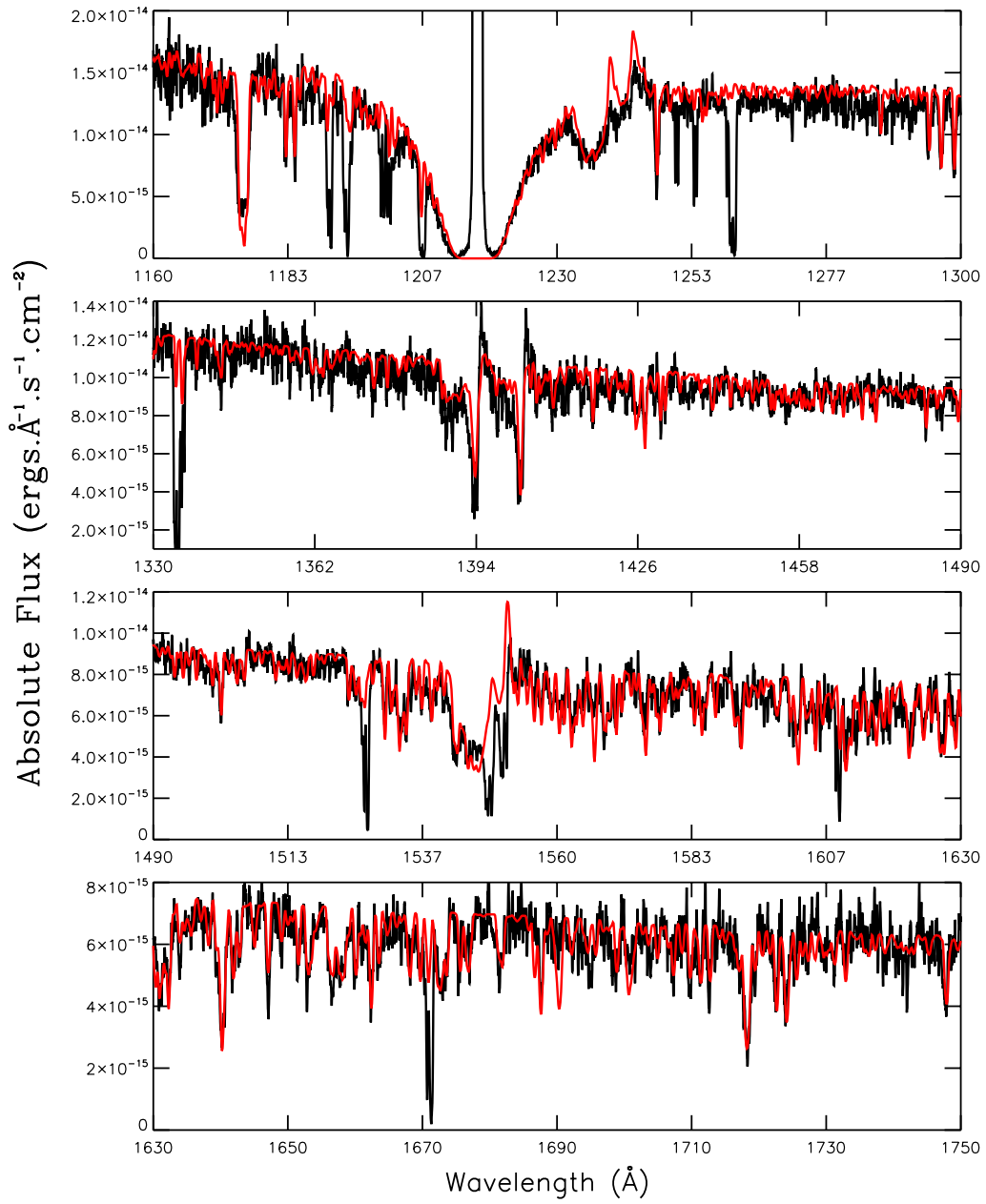


Figure A5. FUV spectrum of IC WLM-A11 (in black). Overplotted in red is the best fit model (see text for comments).

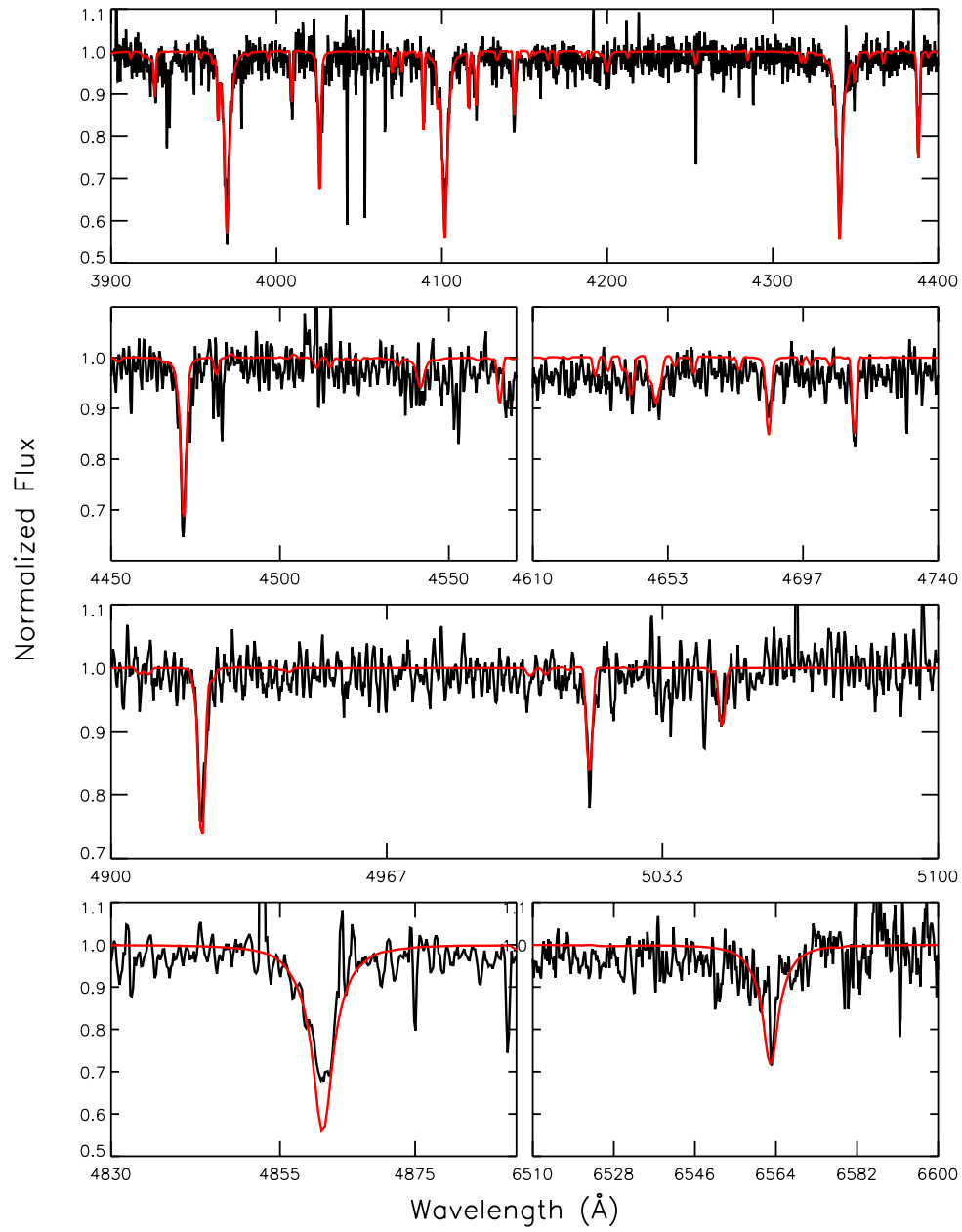


Figure A6. Optical spectrum of WLM-A11. Overplotted in red is the best fit model (see text for comments).